AD-787 509

PATH-LENGTH STABILITY OF THE OCEAN, INFERRED FROM OCEAN TEMPERATURE MEASUREMENTS

D. W. Stowe, et al

Johns Hopkins University

Prepared for:

Advanced Research Projects Agency
Naval Plant Representative Office

May 1974

DISTRIBUTED BY:

NTIS
National Technical Information Service
U. S. DEPARTMENT OF COMMERCE

Unclassified

SECURITY CLASSIFICATION OF THIS PAGE

PLEASE FOLD BACK IF NOT NEEDED FOR BIBLIOGRAPHIC PURPOSES

REPORT DOCUMENTATION PAGE

AD787509

1. REPORT NUMBER
APL/JHU TG 1247

2. GOVT ACCESSION NO

3. RECIPIENT'S CATALOG NUMBER

4. TITLE (and Subtitle)
PATH-LENGTH STABILITY OF THE OCEAN, INFERRED FROM OCEAN TEMPERATURE MEASUREMENTS

5. TYPE OF REPORT & PERIOD COVERED

6. PERFORMING ORG. REPORT NUMBER

7. AUTHOR(s)
D. W. Stowe and F. C. Paddison

8. CONTRACT OR GRANT NUMBER(s)
N00017-72-C-4401
AO 1853

9. PERFORMING ORGANIZATION NAME & ADDRESS
The Johns Hopkins University Applied Physics Laboratory
8621 Georgia Ave.
Silver Spring, Md. 20910

10. PROGRAM ELEMENT, PROJECT, TASK AREA & WORK UNIT NUMBERS

11. CONTROLLING OFFICE NAME & ADDRESS
Naval Plant Representative Office
8621 Georgia Ave.
Silver Spring, Md. 20910

12. REPORT DATE
May 1974

13. NUMBER OF PAGES
~~72~~ 65

14. MONITORING AGENCY NAME & ADDRESS
Naval Plant Representative Office
8621 Georgia Ave.
Silver Spring, Md. 20910

15. SECURITY CLASS. (of this report)
Unclassified

15a. DECLASSIFICATION/DOWNGRADING SCHEDULE

16. DISTRIBUTION STATEMENT (of this Report)
Approved for public release; distribution unlimited.

17. DISTRIBUTION STATEMENT (of the abstract entered in Block 20, if different from Report)

D D C
RECEIVED
MAY 1 1974
C

Reproduced by
NATIONAL TECHNICAL INFORMATION SERVICE
U S Department of Commerce
Springfield VA 22151

18. SUPPLEMENTARY NOTES

19. KEY WORDS (Continue on reverse side if necessary and identify by block number)

Stability	Fluctuations	Sonar
Path-length	Temperature	Synthetic aperture
Phase	Ocean	Sidelooking

20. ABSTRACT (Continue on reverse side if necessary and identify by block number)

In an extensive ocean test at the Atlantic Undersea Test and Evaluation Center (AUTEC), fluctuations of acoustic path length were found to be no more than 0.001 meter rms for periods of 1 minute over a vertical path extending from an ocean depth of 60 to 320 meters. The measurements showed that the ocean is sufficiently stable to allow sophisticated coherent signal processing as would be necessary for synthetic aperture sonar at moderate frequencies (20kHz). Path-length stability was inferred from continuous measurements of the ocean temperature profile determined by a 20-element temperature array suspended from a research vessel. Time-dependent temperature fluctuations remained after the recorded temperature was compensated for changes in depth of the array. These fluctuations were assumed to modulate the sound velocity c, resulting in changes Δl of the acoustic path length l, according to $\Delta l = -l\Delta c/c$.

65

DD FORM 1 JAN 73 1473

Unclassified

SECURITY CLASSIFICATION OF THIS PAGE

TG 1247

MAY 1974

Technical Memorandum

PATH-LENGTH STABILITY OF THE OCEAN, INFERRED FROM OCEAN TEMPERATURE MEASUREMENTS

D. W. STOWE and F. C. PADDISON

SPONSORED BY ARPA UNDER AO 1853

THE JOHNS HOPKINS UNIVERSITY • APPLIED PHYSICS LABORATORY
8621 Georgia Avenue • Silver Spring, Maryland • 20910
Operating under Contract N00017-72-C-4401 with the Department of the Navy

Approved for public release; distribution unlimited.

2

19. KEY WORDS (cont'd)

Medium Stability Experiment
Temperature
Acoustic Signals
Coherent processing

CONTENTS

List of Illustrations 5

1. Introduction 9

2. Configuration of Equipment for Temperature Measurements 13

   Marine Cables and Cable Handling Equipment 13
   Data Monitoring Equipment . . 15

3. Data Processing 19

4. Depth Compensation 21

5. Temperature Error Estimation . . . 29

6. Temperature Data 33

7. Acoustic Path-Length Stability . . . 49

8. Comparison with Other Measurements . . 57

9. Summary and Conclusions 59

   Acknowledgments 61

   References 63

   Appendix: Calculation of Array Configuration . 65

ILLUSTRATIONS

1 Configuration of the Temperature Sensing Array Used During the Medium Stability Experiment . 10

2 Configuration of Equipment Used for Deployment of Temperature Array . . . 14

3 Temperature Gradient Used to Compensate for Changes in Depth During Run 1 . . . 23

4 Temperature Gradient Used to Compensate for Changes in Depth in Post Run 10 Data . . 24

5 Sample Configuration of Temperature Array Derived from Simple Hydrodynamic Theory . 26

6 Maximum Expected Depth Error of Temperature Sensors in Temperature Array . . 31

7 Temperature Data From the Medium Stability Experiment: Sensors 1 Through 8. (Run 1, AUTEC, 30 October 1972; Start Time, 16:17:48Z) 34

8 Temperature Data From the Medium Stability Experiment: Sensors 9 Through 16. (Run 1, AUTEC, 30 October 1972; Start Time, 16: 16:17:48Z) 35

9 Temperature Data From the Medium Stability Experiment: Sensors 17 Through 20. (Run 1, AUTEC, 30 October 1972; Start Time, 16:17:48Z) 36

10 Depth History of Deep Pressure and Shallow Pressure Sensors (Run 1, AUTEC, 30 October 1972) 37

Preceding page blank

THE JOHNS HOPKINS UNIVERSITY
APPLIED PHYSICS LABORATORY
SILVER SPRING, MARYLAND

ILLUSTRATIONS (cont'd)

11 Characteristic Temperature Profiles at AUTEC in October 1972 40

12 Square of Väisälä Frequency at AUTEC Site 1 (4 October 1972, 1800Z) 41

13 Temperature Data from the Medium Stability Experiment: Sensors 1 Through 8. (Post Run 10, AUTEC, 5 November 1972; Start Time, 8:35:52Z) 42

14 Temperature Data from the Medium Stability Experiment: Sensors 9 Through 16. (Post Run 10, AUTEC, 5 November 1972; Start Time, 8:35:52Z) 43

15 Temperature Data from the Medium Stability Experiment: Sensors 17 Through 20. (Post Run 10, AUTEC, 5 November 1972; Start Time, 8:35:52Z) 44

16 Depth History of Deep Pressure and Shallow Pressure Sensors. (Post Run 10, AUTEC, 5 November 1972) 45

17 Typical Temperature History at Sensor 17 (Mean Depth, 271 Meters). (Run 3, AUTEC, 30 October 1972; Start Time, 0:22:52Z) . 48

18 Depth History of Deep Pressure and Shallow Pressure Sensors. (Run 3, AUTEC, 30 October 1972) 48

19 Variation of Acoustic Path, ℓ, with Time Over a 255-Meter Vertical Path. (Run 1, AUTEC, 30 October 1972) 51

ILLUSTRATIONS (cont'd)

20 Standard Deviation of Acoustic Path-Length Fluctuations Computed Over 1-Minute Intervals for a 255-Meter Path. (Run 1, AUTEC, 30 October 1972) . . 51

21 Variation of Acoustic Path, ℓ, with Time Over a 255-Meter Vertical Path. (Post Run 10, AUTEC, 5 November 1972) . . 52

22 Standard Deviation of Acoustic Path-Length Fluctuations Computed Over 1-Minute Intervals for a 255-Meter Path. (Run 1, AUTEC, 5 November 1972) . . 52

23 Variation of Acoustic Path, ℓ, with Time Over a 255-Meter Vertical Path. (Run 3, AUTEC, 30 October 1972) . . 53

24 Standard Deviation of Acoustic Path-Length Fluctuations Computed Over 1-Minute Intervals for a 255-Meter Path. (Run 3, AUTEC, 30 October 1972) . . 53

A-1 Projected Area of a Segment of the Temperature Array 68

A-2 Components of Tension in a Segment of the Temperature Array . . . 70

1. INTRODUCTION

Inhomogeneities in the ocean cause fluctuations of the acoustic path length between the surface and the bottom. Information about these fluctuations is essential for the design of a workable synthetic aperture sonar. In order to gain such information, the Medium Stability Experiment was conducted in the fall of 1972 at the Navy's Atlantic Undersea Test and Evaluation Center (AUTEC) in the Tongue of the Ocean off Andros Island in the Bahamas.

In one phase of the experiment the magnitude of the fluctuations of the acoustic path length was determined, using precise measurements of the travel time of an acoustic pulse propagating from a projector near the ocean surface to an array of bottom-mounted hydrophones. The design, conduct, and results of this aspect of the experiment are detailed in Ref. 1. An extended error analysis with resultant limits on the observed path length stability of the ocean is presented in Ref. 2.

It is the purpose of this report to document the second aspect of this experiment, namely, measurement of ocean temperature profiles in order to estimate acoustic path length stability. In this phase of the experiment, the Applied Physics Laboratory of The Johns Hopkins University measured the temperature of the ocean to a depth of 300 meters. The temperature measurements were obtained with a 300-meter array consisting of 20 thermistors, 2 pressure sensors, and a water velocity meter as shown in Fig. 1. The

---

Ref. 1. A. J. Tardif (ed.), Synthetic Aperture Sonar Medium Stability Experiment, Raytheon Company, Submarine Signal Division, 1973.

Ref. 2. D. W. Stowe, L. H. Wallman, J. W. Follin, Jr., and P. J. Luke, Stability of the Acoustic Path Length of the Ocean Deduced from the Medium Stability Experiment, APL/JHU TG 1230, January 1974.

Preceding page blank

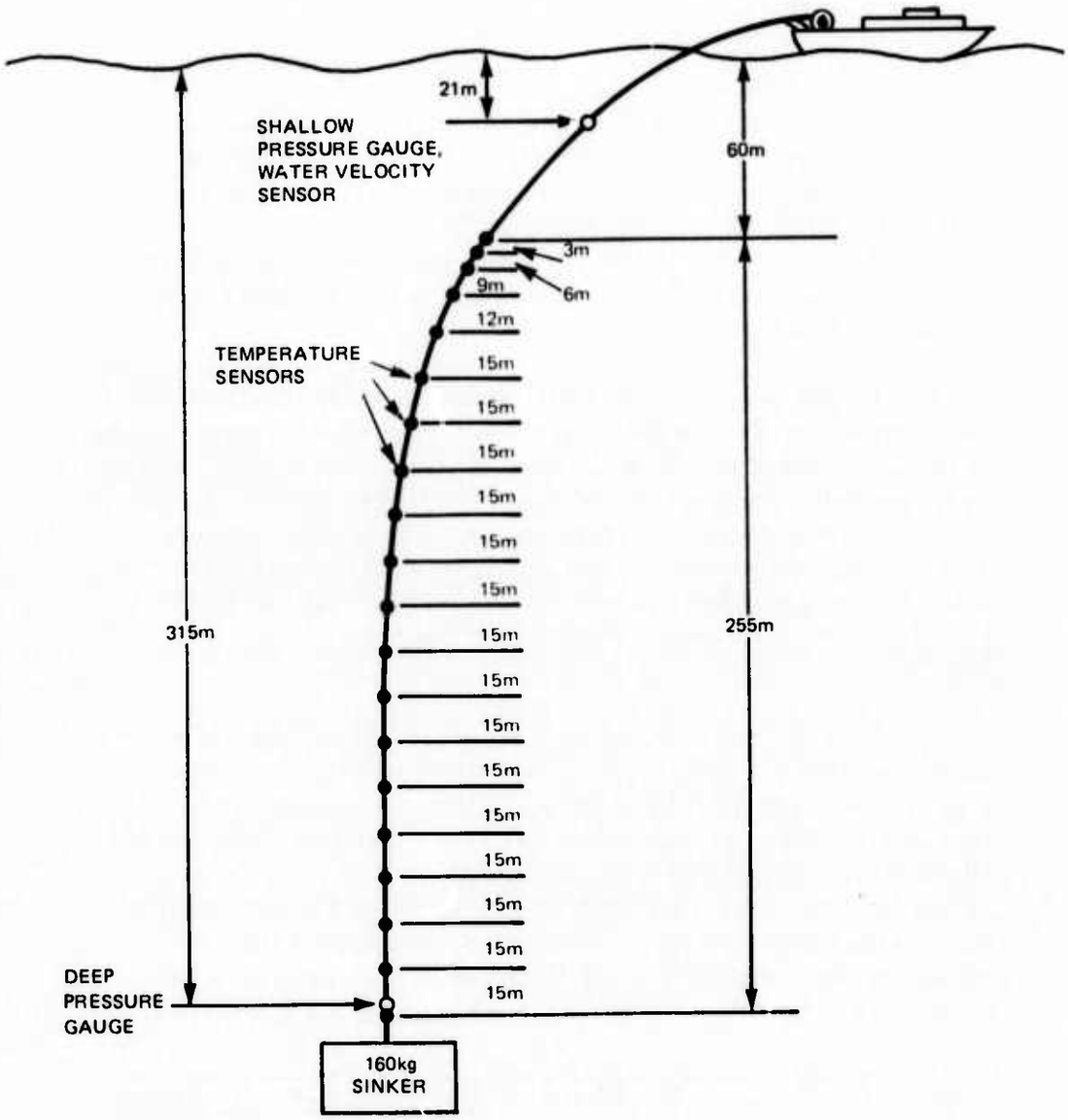

Fig. 1 CONFIGURATION OF THE TEMPERATURE SENSING ARRAY USED DURING THE MEDIUM STABILITY EXPERIMENT

array was suspended from a research vessel that drifted at speeds up to 2 knots during the data sessions. The pressure sensors were used to compensate for variations in depth of the array so that changes in the ocean temperature profile could be measured accurately.

Since changes in the temperature profile are highly correlated with changes in sound velocity, it was possible to deduce from the temperature measurements the magnitude of the fluctuations in acoustic path length. Based on these measurements, typical rms fluctuations in acoustic path length were found to be less than 1 millimeter or $\lambda/150$ for a 10-kHz signal propagating 255 meters from the top to the bottom of the thermistor array.

The technique and equipment used to obtain the temperature measurements are described in substantial detail in Chapter 2 of this report. Data analysis and results are presented in Chapters 3 through 8. A summary of results and conclusions is given in Chapter 9.

2. CONFIGURATION OF EQUIPMENT FOR TEMPERATURE MEASUREMENTS

MARINE CABLES AND CABLE HANDLING EQUIPMENT

A schematic representation of the thermistor array used for gathering data at AUTEC from 16 October to 6 November 1972 is shown in Fig. 1. The array consisted of ten 9.9-millimeter diameter temperature cables from Vector Cable Company of Houston, Texas, ten 5.1-millimeter diameter cables from Hydrolab Company of Austin, Texas, and two pressure cables from Environ-Con Company of Houston, Texas. Each temperature cable terminated in a 2-pin marine connector that mated with a Hydrolab temperature probe. Each pressure cable terminated in four miniature single-pin marine connectors that mated with a strain-gauge pressure sensor. All of the temperature cables, pressure cables, and sensors were pressure tested with a 4-hour soak at 500 psi in a seawater bath prior to shipment to AUTEC. Several faulty terminations were disclosed and repaired.

On the AUTEC research barge, the entire bundle of 22 cables, bound together every meter with nylon cable tie wraps, was stored on a large hydraulic winch. A 0.15-meter layer of cables could be accommodated by the winch across its entire 1-meter width. During deployment, the cables passed over a wooden sheave 1 meter in diameter, at the stern of the barge, as shown in Fig. 2. Below the sheave, the marine cables were tie-wrapped securely to a 4.75-millimeter steel support cable covered with a 1.6-millimeter antiabrasion vinyl jacket. Tie wraps were placed at 2 1/2-meter intervals (the distance from the barge deck to the water line). During the last deployment the tie-wrap spacing was increased to 5 meters without excessive bowing of the marine cables between ties. The temperature and pressure sensors were also tied to the steel cable to prevent streaming of the sensors and to discourage fishbite. As the marine cables were joined to the steel cable, they

Preceding page blank

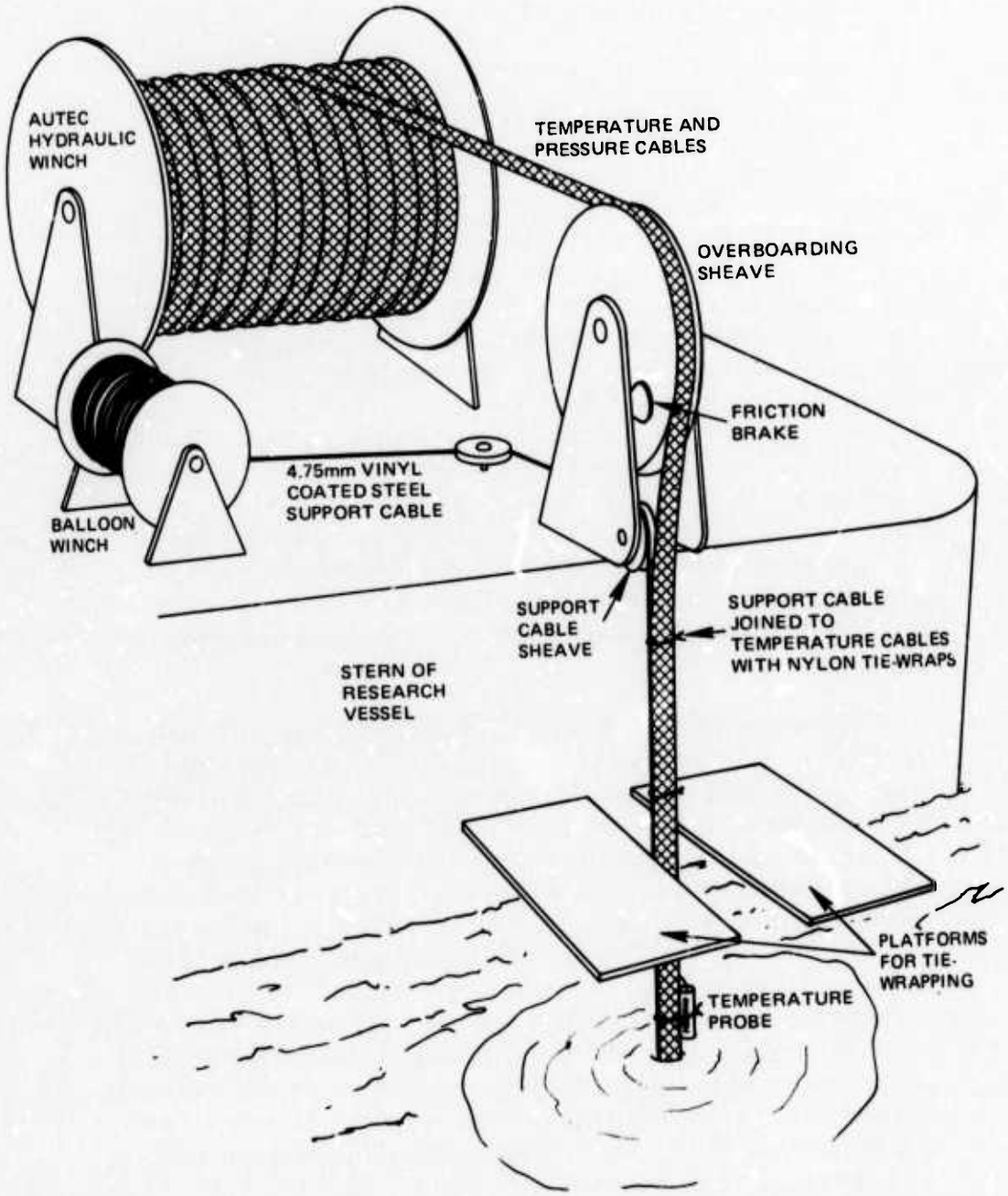

Fig. 2 CONFIGURATION OF EQUIPMENT USED FOR DEPLOYMENT OF TEMPERATURE ARRAY

were kept taut by a brass friction brake sliding on the side of the wooden sheave.

The steel cable that supported most of the weight of the array was stored on an APL/JHU gasoline-driven balloon winch. A 160-kg sinker was attached to the steel cable to lessen streaming of the cable. The steel cable and sinker were lowered to full depth to allow the cable to unwind under tension before deployment with the thermistor cables. During one of the practice deployments, a stabilizing fin was attached to the sinker to prevent twisting. However, the fin and sinker fell to the ocean bottom when a cable clamp worked lose by sliding along the smooth vinyl jacket on the steel cable. Thereafter, the vinyl jacket was removed from the support cable wherever cable clamps were attached. Only a sinker was used on subsequent deployments; nonetheless, twisting of the array remained within manageable limits. The mass of the array was approximately 400 kg, excluding the sinker. A minimum of four men was required for deployment and retrieval. The minimum time required for deployment of the array was 1 hour and 15 minutes and the minimum retrieval time was 52 minutes.

When the array was fully deployed, the arc lengths of the temperature probes measured from the water line were: 61.0, 64.0, 70.1, 79.4, 91.5, 106.7, 121.9, 137.1, 152.3, 167.5, 179.0, 194.1, 209.9, 225.2, 240.8, 256.3, 271.9, 287.7, 303.3, and 318.5 meters. The spacing between the upper five sensors was varied from 3 to 12 meters to obtain a more refined spatial correlation of temperature fluctuations between sensors. Pressure sensors were located at arc lengths of 21.4 and 315.8 meter. A water-velocity gauge measured water velocity parallel and perpendicular to the array at an arc length of 21.3 meters. A fin caused the gauge to align in the direction of the horizontal flow.

DATA MONITORING EQUIPMENT

The temperature cables terminated at the hydraulic winch in MS connectors and were joined to BNC cables

via an MS-to-BNC junction box. The BNC cables and the two pressure cables were connected to a 54-conductor cable via a second junction box. The 54-conductor cable transmitted the signals from the terminus of the array on deck to the instrument room. Two conductors were required for each thermistor and four conductors were required for each pressure sensor. The cable attached to the water current meter went directly to the instrument room.

In the instrument room the temperature cables were terminated at one of two Hydrolab 10S1 scanners. Each scanner could scan 10 sensors at the rate of one per second. The output from each scanner was connected to one of two Hydrolab RT-125 research thermometers. The thermometers measured the combined resistance of the platinum thermistor (nominally, 5000Ω ±25Ω at 25°C), the cable coming from the thermistor (<35Ω) and the solid-state switch in the appropriate scanner channel (≈ 50Ω). The thermometer provided a linear voltage (0 to 100 mVdc, full scale) proportional to the temperature determined from the thermistor resistance. The outputs of the two research thermometers were amplified by solid-state operational amplifiers (gain = 16) and recorded on two tracks of a 14-track Ampex FR 1300.

Each temperature probe consisted of a platinum thermistor encased in a glass tube. A protective plastic cylinder encircled the glass tube at a distance of a centimeter, which was sufficient to allow circulation of seawater around the temperature-sensitive region. The 1/e response time of the probes was about 3 1/2 seconds. The detailed relationship between resistance and temperature as supplied by the manufacturer, Fenwal Electronics, Framingham, Mass., is given in Table 1. The tolerance of the thermistors was rated at ±1/2% of the 5000Ω nominal resistance at 25°C. Consequently, the absolute accuracy of the temperature measurements is only several tenths of a centigrade degree, including the effects of cable resistance and switching networks. However, since the temperature coefficients of the cable resistance and switching networks are small, measurements

Table 1

Resistance of Platinum Thermistors
as a Function of Temperature

Temperature (°C)	Resistance (Ω)	Temperature (°C)	Resistance (Ω)
10	9950	21	5972
11	9485	22	5710
12	9045	23	5462
13	8627	24	5225
14	8232	25	5000
15	7855	26	4787
16	7500	27	4583
17	7162	28	4388
18	6840	29	4205
19	6535	30	4028
20	6247	31	3862

of relative changes in temperature are accurate to 10% of the temperature change, corresponding to accuracies on the order of 0.02°C or less.

The pressure gauges were of the strain-gauge type. A stable 10.00 Vdc power supply provided the reference voltage for the Wheatstone bridge configuration of sensing elements in the pressure gauge. The outputs of the pressure gauges (~0 to 40 mVdc, full scale) were amplified with a gain of 64 and recorded on the FR 1300. The pressure gauges were calibrated in the laboratory before and after the experiment, and no changes in the gauge characteristics were noted. Based on the laboratory calibrations, the relative accuracy of both the shallow and deep pressure sensors was ±0.3 meter.

THE JOHNS HOPKINS UNIVERSITY
APPLIED PHYSICS LABORATORY
SILVER SPRING, MARYLAND

The outputs of the horizontal and vertical channels of the Marsh McBirney water current meter were recorded directly on the FR 1300 without amplification. At present, no analysis of the water velocity data has been undertaken other than to provide an estimate of the ship's drift velocity.

The demodulated outputs from the FR 1300 playback heads for the two temperature tracks, the two pressure tracks, and the vertical water velocity track were monitored successively, two at a time, on a Sanborn strip-chart recorder. This arrangement permitted a rapid check that the entire system was functioning properly and provided a permanent analog record of each data run. Since a sixth demodulator was not available, the output of the horizontal water-velocity gauge, rather than the demodulated recorder playback, was recorded on the Sanborn recorder.

At 4- to 5-minute intervals calibrations were placed on each tape track to enable later compensation of the data for drift in the electronics. Zero and full-scale voltages of the temperature channels were obtained by switching the research thermometers to the internal calibration settings. The pressure channels were calibrated at three voltage levels provided by a stable voltage source. The water-velocity meter contained an internal half-scale calibration of both velocity channels. The zero of the vertical velocity channel can be determined by requiring that the time-averaged velocity of that channel be zero. A Weston digital voltmeter was used as the standard voltage reference for calibration voltages.

The center frequency of the Ampex FR 1300 was 27 kHz for a tape speed of 15 ips. A stable reference frequency of 25 kHz was recorded in order to compensate for variations in tape speed. In addition, a voice channel and IRIG B time code were recorded. Spot checks of the reference frequency and IRIG B channels were made during data runs with an oscilloscope to assure proper operation. Each of the six oceanographic data channels was recorded on FM tracks.

3. DATA PROCESSING

Data from the temperature sensors, pressure gauges, and current meter were recorded in analog form on magnetic tape. Output from the pressure gauges and from each axis of the current meter were recorded continuously. However, the output from a given temperature sensor was recorded for about 1 second out of 11 owing to the necessity of scanning from thermistor to thermistor. The scanners were free-running, but dwelled twice as long on the first channel as on other channels to provide a means of channel identification.

The data tapes were digitized at APL/JHU by the Instrumentation Development Group. An 11-bit A-to-D converter was used to digitize the data. The conversion gains were adjusted so that the full range of analog valves on a given channel was approximately 1/4 of full scale on the converter. This adjustment eliminated conversion problems caused by switching of the temperature scanners and provided a least significant bit equal to 0.2% of the full scale analog voltage.

During the data digitization process each tape track was sampled at an effective rate of 25 samples per second. The scan period of the scanners on the temperature channels was sufficiently constant over a 10-minute period that the transition between thermistors could be predicted to within ±3 samples by counting the number of samples since the start of the run. In this manner, the middle 15 samples of a thermistor were selected and averaged to provide the value of the temperature of a given thermistor on a particular scan. The least significant bit of the digitized data was approximately 0.02°C. The standard deviation of the digitized samples during a single scan of a thermistor was on the order of 0.015°C to 0.02°C. Since the response time of the temperature sensors was 3 1/2 seconds, this rms scatter is

due solely to measurement noise. The standard deviation of the mean of the 15-point sample is smaller by a factor of $\sqrt{15}$ (Ref. 3) and is equal to 0.005°C rms or less.

Temperature data have been processed for times corresponding to Runs 1 and 3 of the acoustic portion (Refs. 1 and 2) of the Medium Stability Experiment. Additional temperature data were processed for a 50-minute interval following acoustic Run 10 on 5 November 1973.

Ref. 3. A. Hald, Statistical Theory with Engineering Applications, John Wiley and Sons, Inc., New York, 1965, p. 199.

4. DEPTH COMPENSATION

During the Medium Stability Experiment, changes in the speed and direction of the research vessel caused the hydrodynamic drag acting on the temperature array to vary. This variation of the drag caused corresponding changes in the shape and depth of the array. Consequently, it was necessary to compensate the temperature measurements for changes in depth of the array. The compensated temperature corresponds to the temperature that would be recorded by a sensor held at constant depth.

The temperature T recorded by a temperature sensor at depth z is related to the temperature T_o at the reference depth z_o by the local temperature gradient $\frac{dT}{dz}(z)$ according to the expression,

$$T = T_o + \int_{z_o}^{z} \frac{dT}{dz}, dz'. \tag{1}$$

To calculate changes in acoustic path length, it is desirable to know the temperature at a reference depth as a function of time. When the depth variation of the array during a data run was less than the 15-meter maximum spacing between temperature sensors, the first term of the expansion of the integral in Eq. 1 can be used to approximate the reference temperature T_o at depth z_o,

$$T_{o_i} = T_i - \left(\frac{dT}{dz}\right)_i \cdot (z_i - z_{o_i}), \tag{2}$$

where T_i is the uncompensated temperature recorded by the ith temperature sensor and $(\frac{dT}{dz})_i$ is the local temperature gradient. An empirical value of the gradient is chosen by taking that value which minimizes or eliminates features in the temperature history of each sensor that correlate with similar distinctive features in the depth history of the same sensor. A single value of the gradient is used for each sensor during a data run.

The gradients that were used to compensate the Run-1 and post Run-10 temperature data are shown in Figs. 3 and 4. The solid curves are merely visual aids connecting the point values of the empirical gradients. The gradients are seen to fluctuate wildly as a function of depth, indicating that the approximation that dT/dz is independent of depth in the vicinity of a given sensor is not rigorous. The depth-corrected temperatures calculated from Eq. 2 will contain additional errors if the true ocean gradient varies with time or if it varies in the horizontal plane as the array translates with the research vessel.

In order to infer the depth of the individual temperature sensors, it is necessary to know the shape and depth of the array when it is fully deployed. A model for the shape of the array has been derived in the Appendix, based on the assumption that the upper end of the array is affixed to the research vessel which moves with a constant velocity v through motionless water. The density of the array is assumed to be the same as that of seawater and a drag-free sinker is assumed to be attached to the bottom of the array. Using a simple form for the hydrodynamic drag on a cable of uniform diameter, it is shown in the Appendix that the shape of the array approximates a parabola, i.e., $x - x_{bottom} = B(z - z_{bottom})^2$. The variable x represents horizontal displacement, z is the depth coordinate, the subscript "bottom" denotes the bottom of the array, and B is a coefficient that is a function of the drag force and the weight of

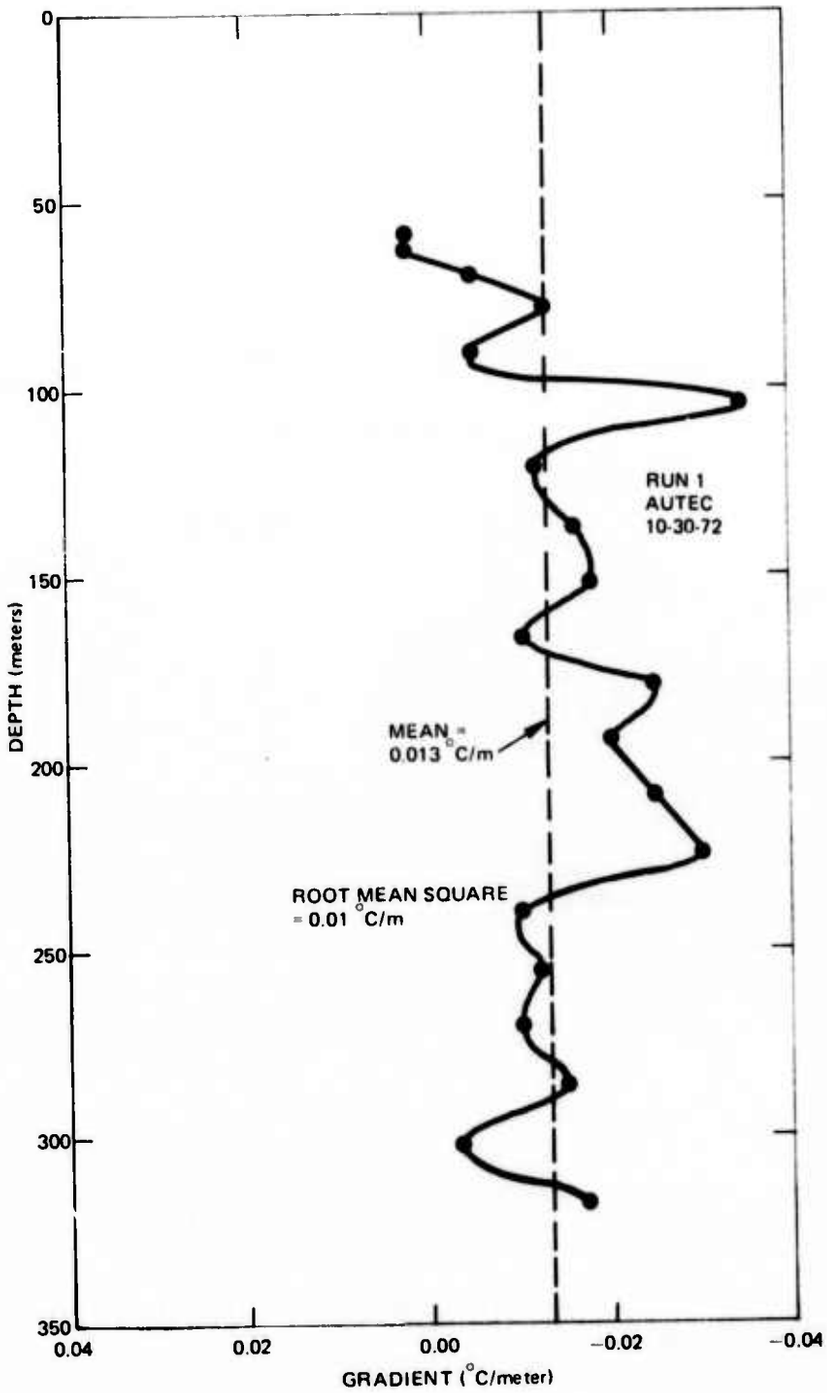

Fig. 3 TEMPERATURE GRADIENT USED TO COMPENSATE FOR CHANGES IN DEPTH DURING RUN 1

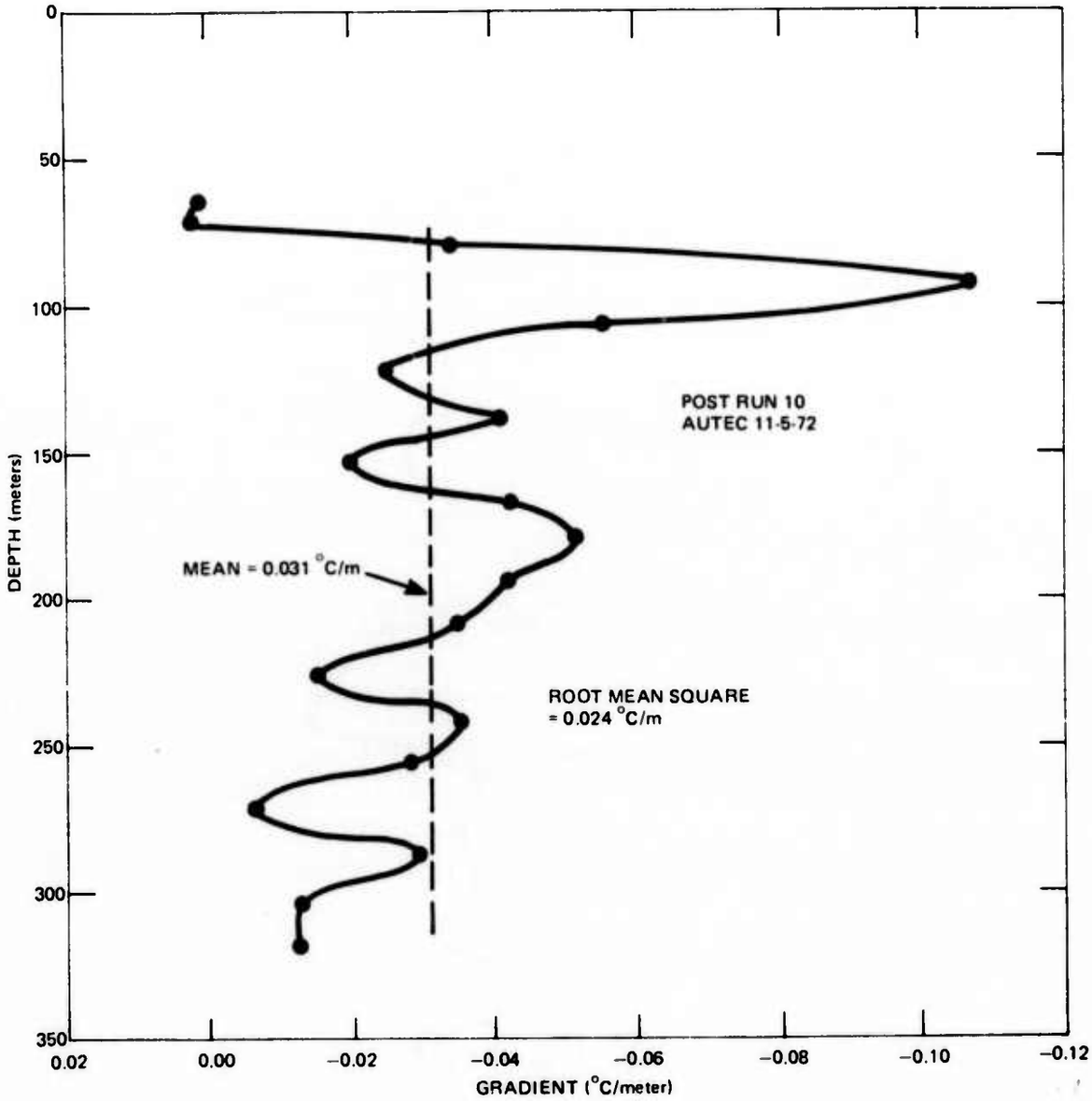

Fig. 4 TEMPERATURE GRADIENT USED TO COMPENSATE FOR CHANGES IN DEPTH IN POST RUN 10 DATA

the sinker. The form and magnitude of the drag coefficient was obtained from Ref. 4. A typical configuration of the array is shown in Fig. 5.

The model used to calculate the array shape can be refined to include taper of the array. This configuration can occur because there are fewer cables near the bottom of the array then near the top. The equations for the tapered array are also derived in the Appendix and a numerical solution is shown in Fig. 5.

The array has the form of a vertical line when the difference in depth between the deep and shallow pressure sensors is equal to the arc length of the cable between them. As the depth separation between the two sensors decreases, the array takes the form of a parabola with its curvature increasing as the depth separation decreases. Once the shape of the array is known, the depth of an individual temperature sensor is found by integrating the arc length up the array until the depth is reached at which the arc length along the array is equal to the arc length to the given temperature sensor.

The calculation of sensor depths does not account for irregularities in the shape of the array caused by ocean currents that are nonuniform across the array. The calculation also does not account for the transient behavior of the array following maneuvers of the research vessel. Additional pressure sensors distributed along the array would have enabled compensation for these effects.

During Run 3 the depth of the bottom of the array varied by 30 meters, twice the spacing between temperature sensors, because of changes in the course of the research vessel. Consequently, the constant temperature-gradient approximation was not valid for these data, so an alternative technique was used to compensate these data for changes in

---

Ref. 4 H. Schlichting, Boundary Layer Theory (6th Edition), McGraw-Hill Book Co., New York, 1968, pp. 9-16.

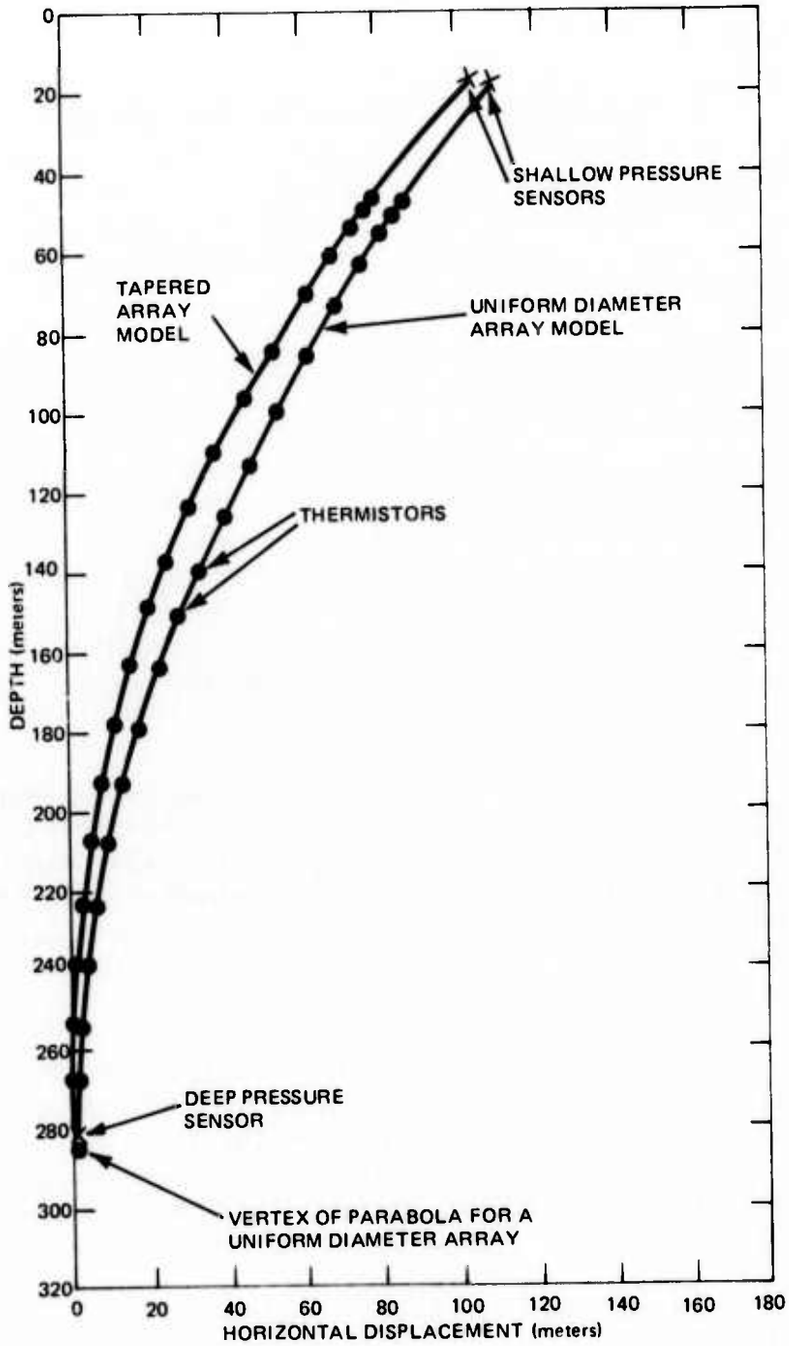

Fig. 5 SAMPLE CONFIGURATION OF TEMPERATURE ARRAY DERIVED FROM SIMPLE HYDRODYNAMIC THEORY

depth of the array. As a function of time the temperature recorded by a sensor and its corresponding depth are known within experimental error. In order to derive the compensated temperature at some reference depth, the temperatures recorded by the 20 temperature sensors were fit with a spline curve as a function of depth. At the reference depth the value assumed by the spline profile is used as the compensated temperature. A spline profile consists of a cubic arc between adjacent points such that the arcs between successive points and the first and second derivatives are continuous along the profile (Ref. 5). Furthermore, to uniquely define the arcs, the second derivative at the top and bottom points are assumed to be zero. A new spline profile is calculated each time a compensated temperature is computed.

Ref. 5. J. H. Ahlberg, E. N. Nilson, and J. L. Walsh, The Theory of Splines and Their Applications, Academic Press, New York, 1967.

5. TEMPERATURE ERROR ESTIMATION

Fluctuations in acoustic path length are proportional to fluctuations of the depth-compensated temperature T_o about its mean value $\langle T_o \rangle$. Consequently, in order to establish confidence in the acoustic path length derived from the temperature measurements, it is necessary to establish error limits on the fluctuation of the compensated temperature. It follows from Eq. 2 that errors in temperature fluctuations $\epsilon(T_o - \langle T_o \rangle)$ can be approximated by

$$\epsilon(T_o - \langle T_o \rangle) \approx |\epsilon(T - \langle T_o \rangle)| + |\Delta z \epsilon(\frac{dT}{dz})| + |\frac{dT}{dz} \epsilon(\Delta z)|, \quad (3)$$

where T is the uncompensated temperature, $\Delta z = z - z_o$ is the change in depth, and ϵ represents the error in the associated quantity. Errors in the temperature gradient are correlated somewhat with errors in depth, so this expression is not exact; it is merely an indication of the upper bound to be placed on measurement errors contained in the data.

Errors in the recorded temperature fluctuation $\epsilon(T - \langle T_o \rangle)$ are on the order of 0.005°C rms, which is the standard deviation of the average temperature during a thermistor scan. For want of a better estimate, errors in the empirical temperature gradient $\epsilon(\frac{dT}{dz})$ are assumed to be 1/4 of the standard deviation of the observed gradient from its mean value. The standard deviation of the gradient in the post-Run 10 data is 0.024°C/m (Fig. 4), which is larger than the value from Run 1 (Fig. 3). Based on a standard deviation of 0.024°C/m, the error $\epsilon(dT/dz)$ is estimated to be 0.006C/m rms. In the data from Run 1 and post-Run 10, the relative depth of the array varied less than 6 meters for the most part, so the standard deviation of the errors arising from the term $\Delta z \epsilon(dT/dz)$ in Eq. 3 are no more than 0.036°C.

Preceding page blank

Estimating the accuracy of the thermistor depths derived from the pressure sensor data is difficult. Based on laboratory calibrations and on the sensitivity of the A-to-D converter, measurement errors in the depths of the pressure sensors themselves are less than 0.3 meter and do not contribute significantly to errors in the estimated depths of the thermistors. The dominant errors arise when the thermistor depths are interpolated from the pressure sensor depths. These errors are estimated by assuming that the true shape of the temperature array differed no more from the tapered array model than the tapered array model differs from the uniform array model as discussed in Chapter 4. In other words, higher order corrections to the simplified hydrodynamic equations derived in the Appendix for the shape of a uniform-diameter array are assumed to have no greater effect than the correction for array taper.

When the array is vertical, both models predict the identical depth for a given thermistor. However, as the depth separation between deep and shallow pressure sensors decreases, the depths predicted by the two models begin to diverge. During the Medium Stability Experiment, the depth separation between the pressure sensors is rarely less than 90% of the cable length between the sensors. The calculations shown in Fig. 5 represent the limiting case where the pressure sensors are separated by about 90% of the cable length between them. Thus, the differences in depth of a given sensor predicted by the two models in Fig. 5 is the maximum depth error expected in the Medium Stability data. This maximum expected depth error is shown in Fig. 6 and and has an rms value of 1.7 meters when calculated over all sensors. If the depth separation between pressure sensors varies by only a few percent of the cable length, rather than 10%, the error in relative depth of a given thermistor will be less than the maximum depth error for that thermistor. A typical temperature gradient of 0.022°C/meter is obtained by averaging data from Run 1 and post-Run 10 (Figs. 3 and 4). The resultant error contributions from the final term

$\frac{dT}{dz} \epsilon(\Delta z)$ in Eq. 3 are found to be on the order of 0.037°C

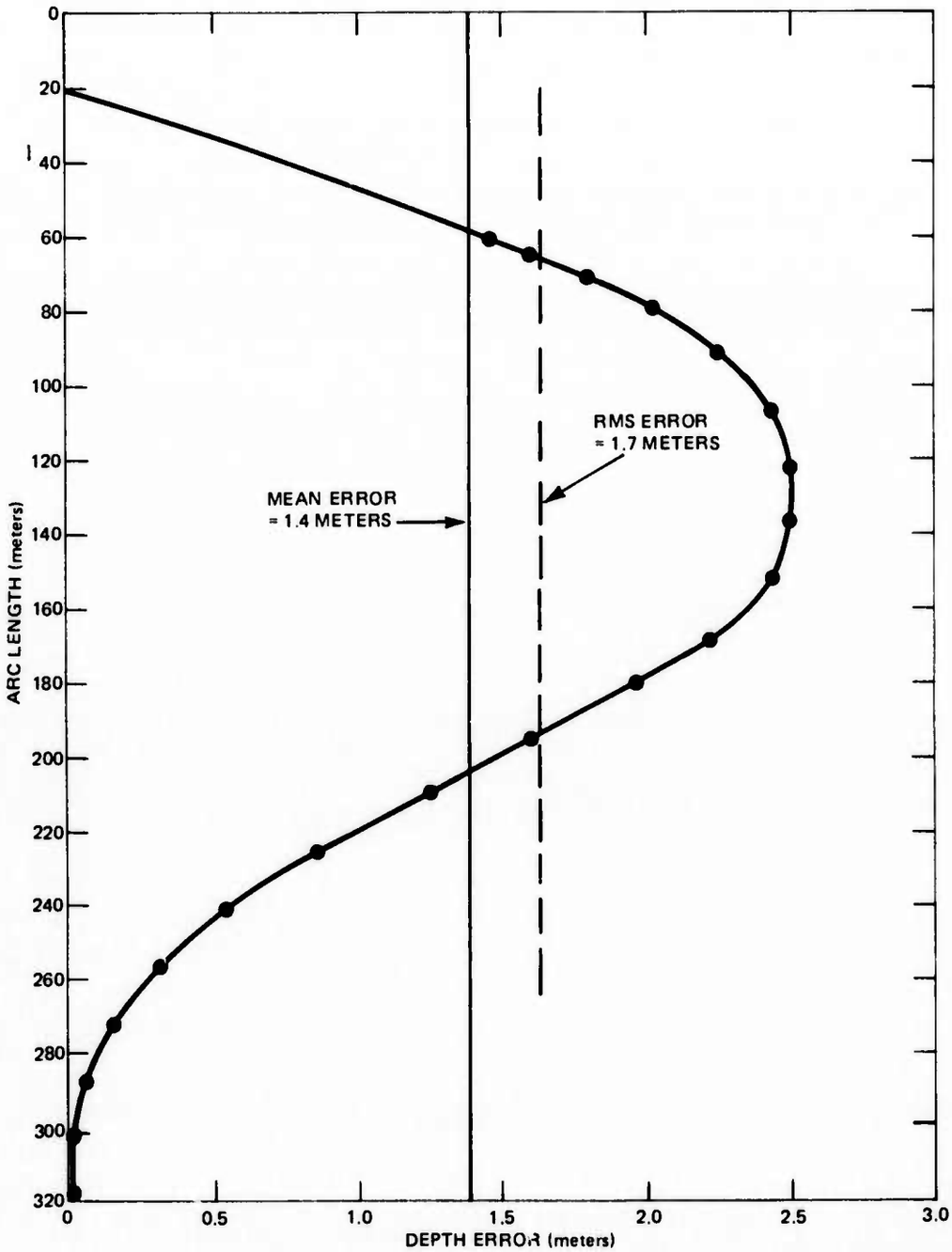

Fig. 6 MAXIMUM EXPECTED DEPTH ERROR OF TEMPERATURE SENSORS IN TEMPERATURE ARRAY

rms. Summing the three error terms in Eq. 3 yields an estimate of measurement errors equal to 0.08°C rms. Thus, the temperature error between any two temperature measurements during the entire run is typically on the order of 0.08°C.

However, relative errors in the temperature over periods on the order of 1 minute are also of interest. During much of the temperature data, the depth of the bottom of the array varies no more than 0.5 meters during a minute's time. In this case, the last two error terms in Eq. 3 contribute less than the 0.005°C rms scatter observed from scan to scan on each temperature channel.

6. TEMPERATURE DATA

The temperature data from Run 1 are shown in Figs. 7 through 9 and the corresponding pressure data are shown in Fig. 10. The depth-compensated temperature is shown as a solid line and the uncompensated temperature is shown as a series of dots when it differs significantly from the compensated temperature. The pronounced spikes in the temperature data at 6.5 minutes on sensors 1, 8, 9, and 10 occurred because the data processing routine did not synchronize properly with the temperature scanner.

The temperature histories displayed in this report were obtained by interpolating among the recorded temperature data. An independent temperature reading from each sensor was obtained only once every 11 seconds, so a linear interpolation between successive readings of a given sensor was used to obtain simultaneous values for the temperature of all sensors once every 4 seconds.

The Run 1 data were taken before noon on 30 October 1972 in seas that were glassy calm with a breeze less than 5 knots. The speed of the research vessel through the water was about 0.5 knot during most of the run. The depth variations of the array represented in Fig. 10 result from variations of the hydrodynamic drag caused by maneuvers of the research vessel. Note that the depth of the bottom of the array increased 3 meters during the run whereas the depth of the shallow pressure sensor only varied 0.3 meter about its nominal depth of 21 meters. This behavior is characteristic of the array as its curvature increases or decreases.

Several features of the depth profile are reflected in the temperature data. For instance, the rapid increase in array depth occurring between minutes 2 and 4 manifests itself in a hump in the compensated temperature profiles of sensors 1, 2, and 14. Evidently the temperature gradients in the vicinity of these sensors were not adequately represented by a constant value.

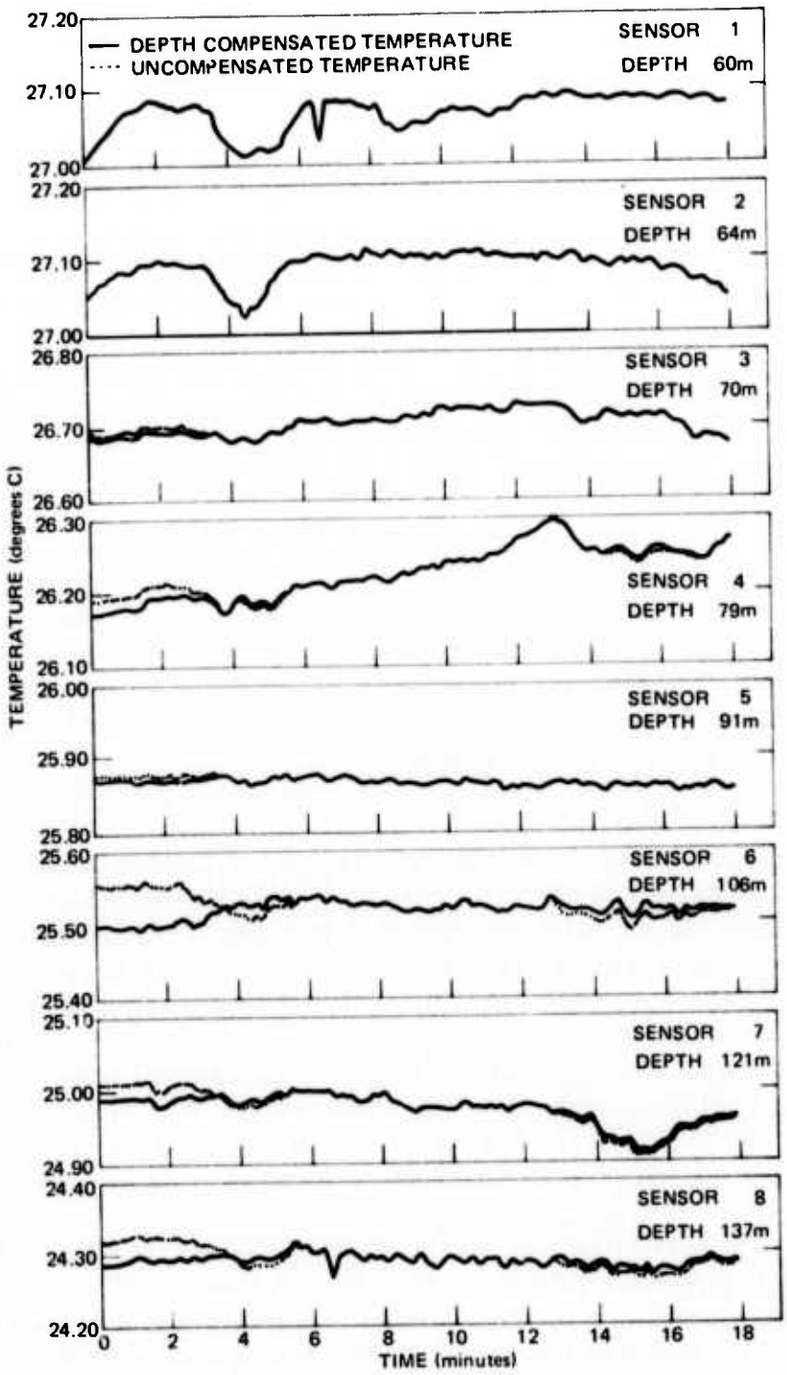

Fig. 7 TEMPERATURE DATA FROM THE MEDIUM STABILITY EXPERIMENT: SENSORS 1 THROUGH 8. (RUN 1, AUTEC, 30 OCTOBER 1972; START TIME, 16:17:48Z)

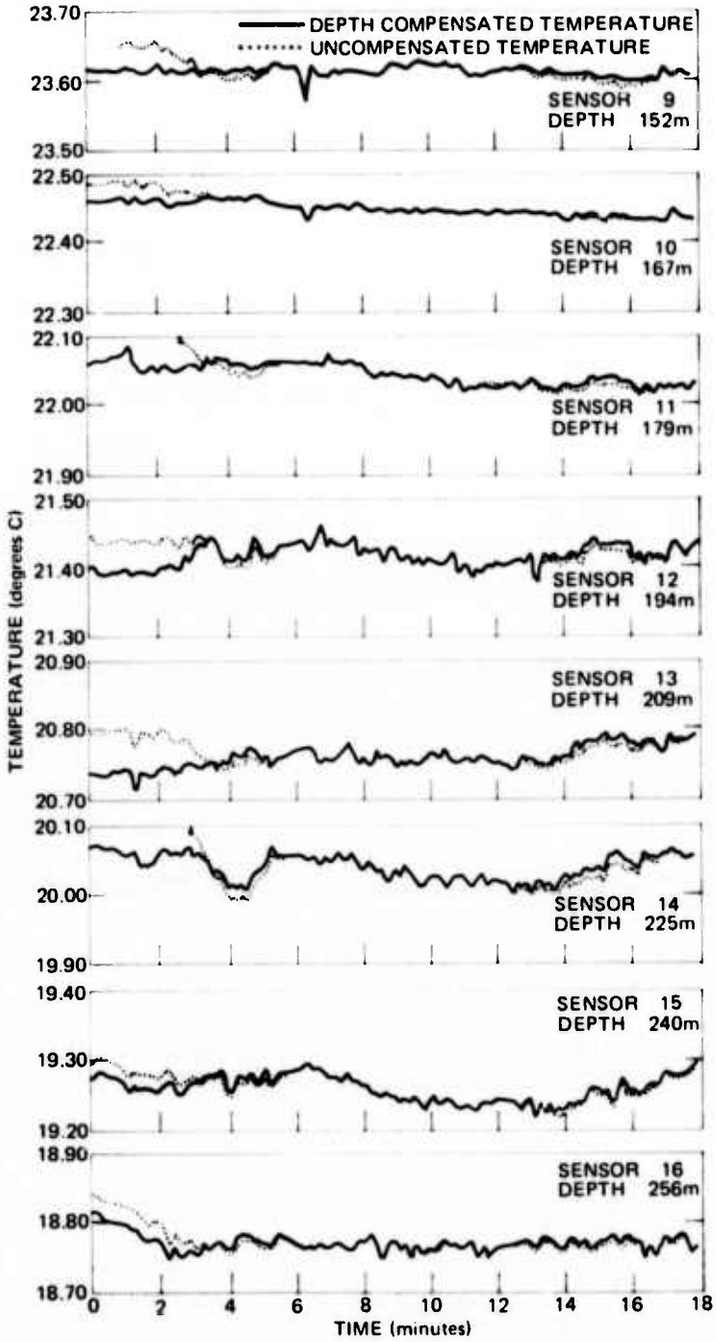

Fig. 8 TEMPERATURE DATA FROM THE MEDIUM STABILITY EXPERIMENT: SENSORS 9 THROUGH 16. (RUN 1, AUTEC, 30 OCTOBER 1972; START TIME, 16:17:48Z)

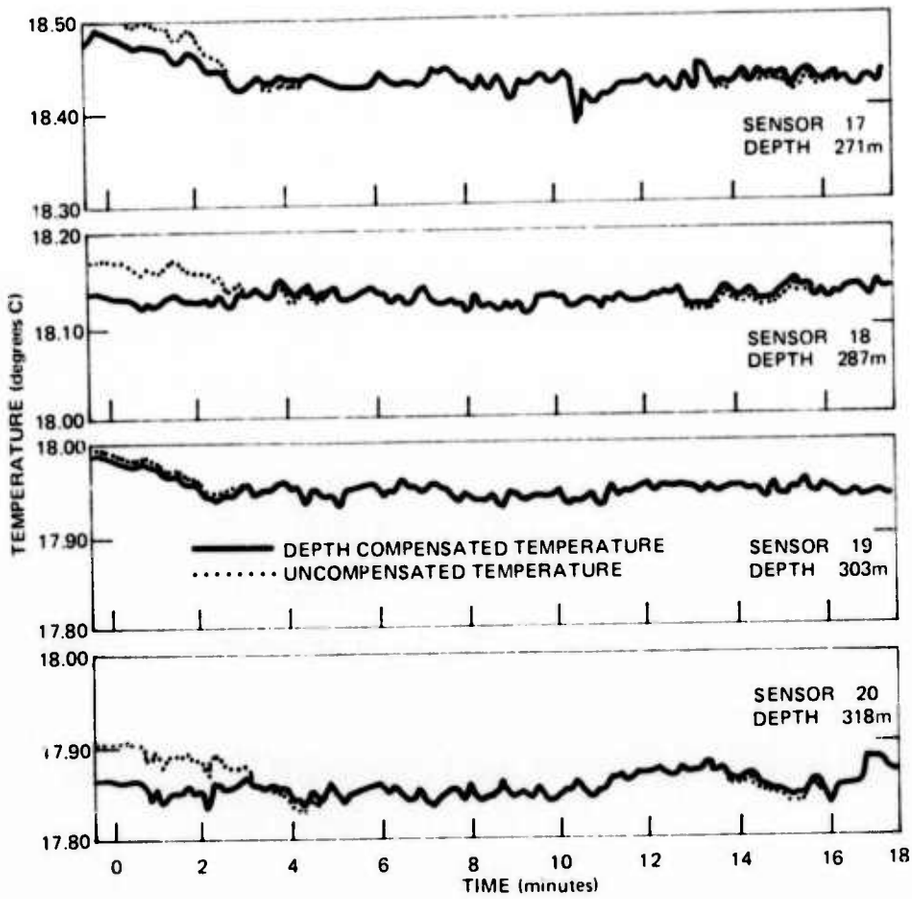

Fig. 9 TEMPERATURE DATA FROM THE MEDIUM STABILITY EXPERIMENT: SENSORS 17 THROUGH 20. (RUN 1, AUTEC, 30 OCTOBER 1972; START TIME, 16:17:48Z)

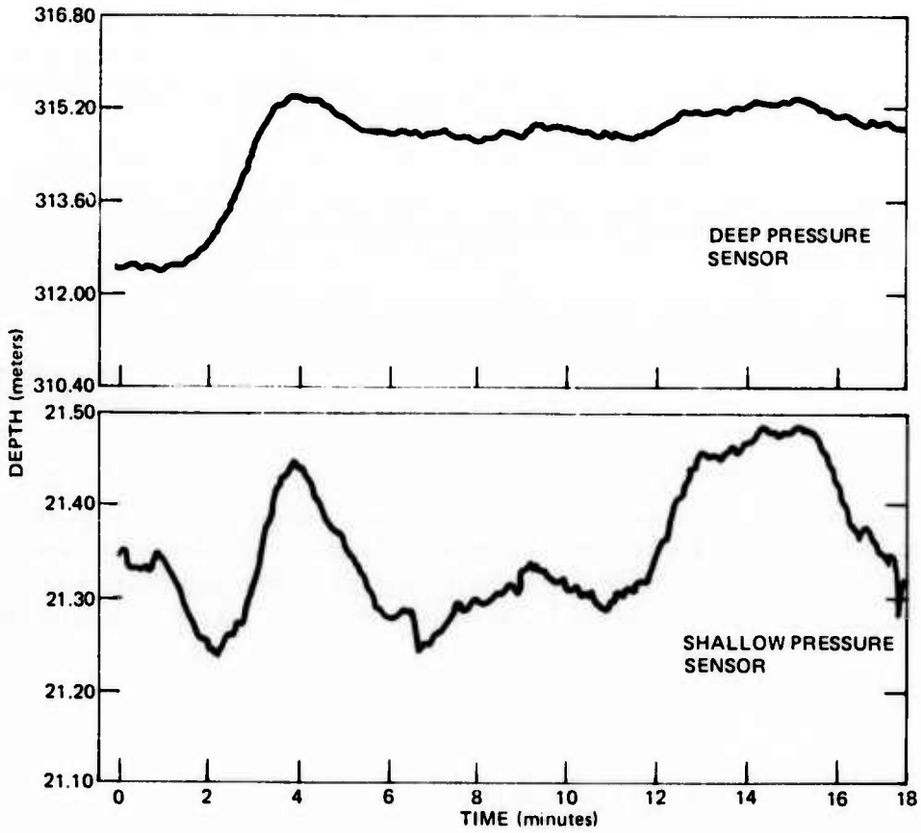

Fig. 10 DEPTH HISTORY OF DEEP PRESSURE AND SHALLOW PRESSURE SENSORS (RUN 1, AUTEC, 30 OCTOBER 1972)

During the 18 minutes of Run 1 most of the sensors indicated a temperature that was constant within several hundredths of a centigrade degree. However, most of the temperature fluctuations with periods of 30 seconds or less are larger than the 0.005°C rms standard deviation of the processing noise. These fluctuations may have been caused by small horizontal gradients (patches) in the ocean that were encountered as the research vessel pulled the array through the water. Alternatively, small changes in depth, perhaps less than the 1-foot resolution of the depth sensors, may have carried the temperature sensors into adjacent microstructure layers with corresponding changes in temperature.

No unequivocal evidence of internal waves was obtained during the experiment; however, the temperatures recorded on sensors 12 through 15 do show a low amplitude oscillation with a 10-minute period which could be a manifestation of either internal waves or measurement errors. In either case, the amplitude of the oscillation is not sufficient to affect the acoustic path length stability during typical synthetic aperture processing times on the order of 1 minute.

According to basic hydrodynamic theory, no internal waves with periods less than 7 minutes were to be expected during the Medium Stability Experiment. As shown in Ref. 6, the Brünt-Väisälä frequency $f_{BV}(z)$ is the maximum frequency at which internal waves can exist. This frequency is a function of the local density and density gradient and is given by

$$f_{BV}(z) = \frac{1}{2\pi}\left(\frac{g}{\rho_o}\frac{\partial\bar{\rho}}{\partial z}\right)^{1/2},$$

where g is the earth's gravitational acceleration, z is the depth, ρ_o is the mean density, and $\partial\bar{\rho}/\partial z$ is the mean gradient in the vicinity of the internal wave.

Ref. 6. O. M. Phillips, The Dynamics of the Upper Ocean, Cambridge University Press, Cambridge, Mass., 1966, p. 162.

The characteristic Brünt-Väisälä frequency for the Medium Stability Experiment has been calculated by Dr. D. Wenstrand of APL. In this calculation he used the temperature profile from an XBT cast to calculate the local seawater density and gradient. The XBT cast, which is shown in Fig. 11, was taken at AUTEC 3 weeks prior to the Medium Stability Experiment and is similar to the accompanying temperature profile obtained with the thermistor array during Run 1. In addition to the temperature profile, a standard salinity profile appropriate to the location and time of year was used to determine the local seawater density. The local density gradient was obtained by calculating the least squares fit of the density to a straight line for 10 meters above and below the depth in question.

The results of these calculations, the square of the Väisälä frequency, is shown in Fig. 12. The maximum frequency occurs in the sharp thermocline just below the mixed layer and corresponds to wave periods of 7 minutes. At the 200- and 250-meter depth of the long period oscillations observed in Run 1 the internal wave periods should be no less than 9 to 10 minutes. Since the observed oscillations had periods on the order of 10 minutes, it is possible, but by no means certain, that they were caused by low amplitude internal waves.

The decreased spacing between the upper five sensors of the array was intended to provide a more refined measure of the spatial correlation of temperature variations. However, since the temperature fluctuations in the AUTEC measurements are so small, they are dominated by measurement noise. Consequently, the spatial correlation of the temperature measurements between the uppermost sensors appears to be no more than between any two adjacent sensors in the array.

Additional temperature data were taken for 1 1/2 hours following acoustic Run 10 of the Medium Stability Experiment. Fifty minutes of these data were processed and are shown in Figs. 13 through 16. The data were taken

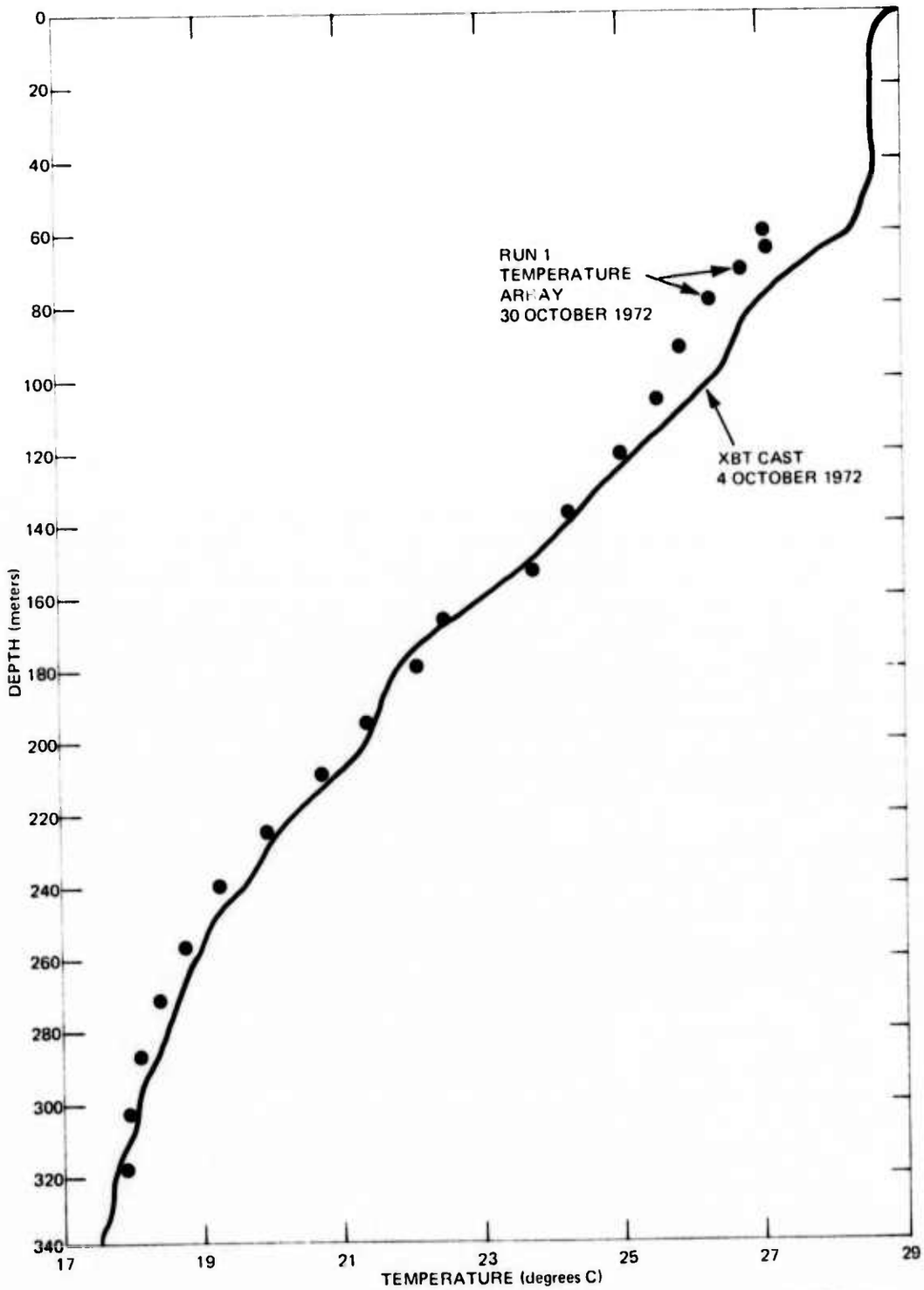

Fig. 11 CHARACTERISTIC TEMPERATURE PROFILES AT AUTEC IN OCTOBER 1972

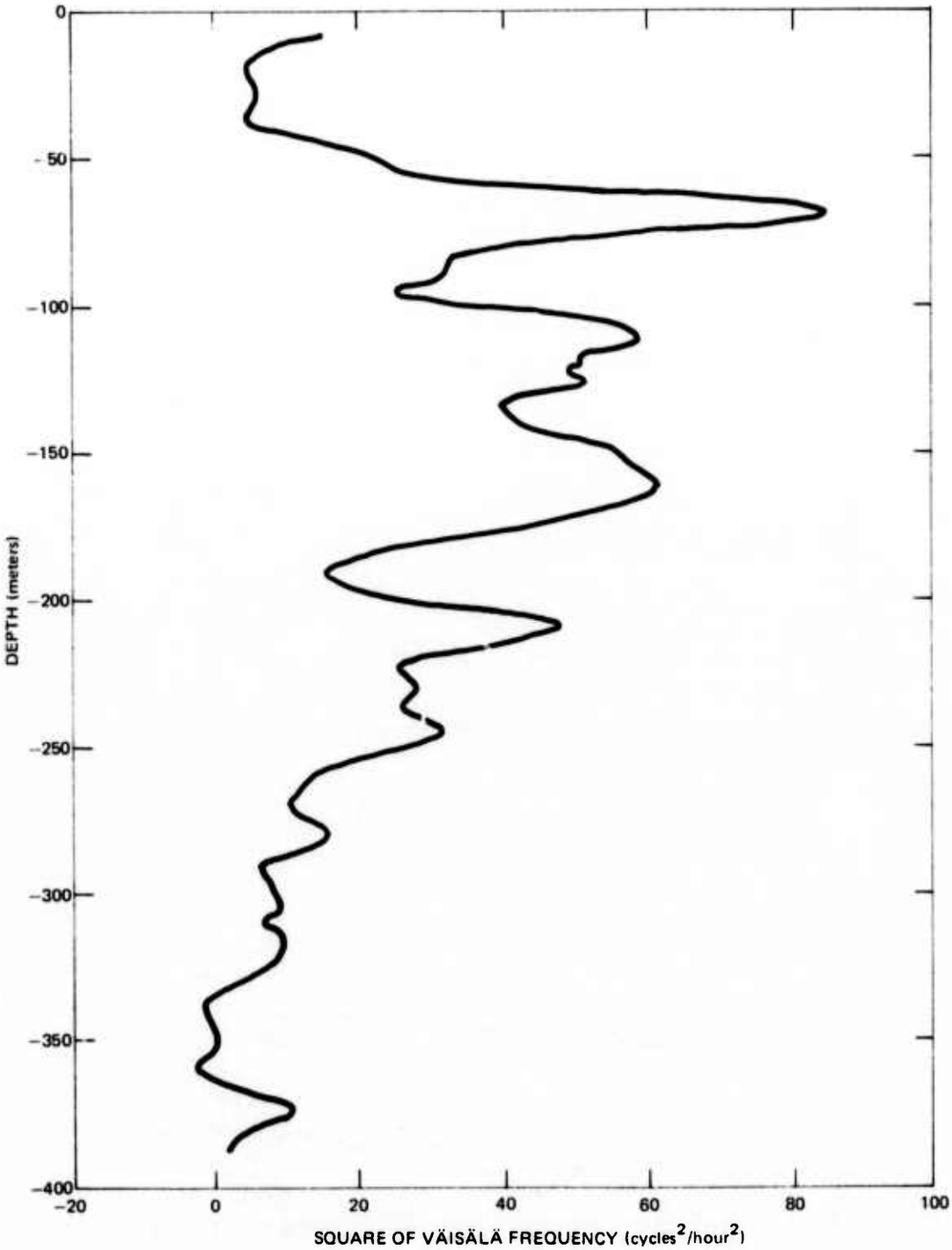

Fig. 12 SQUARE OF VÄISÄLÄ FREQUENCY AT AUTEC SITE 1 (4 OCTOBER 1972, 1800Z)

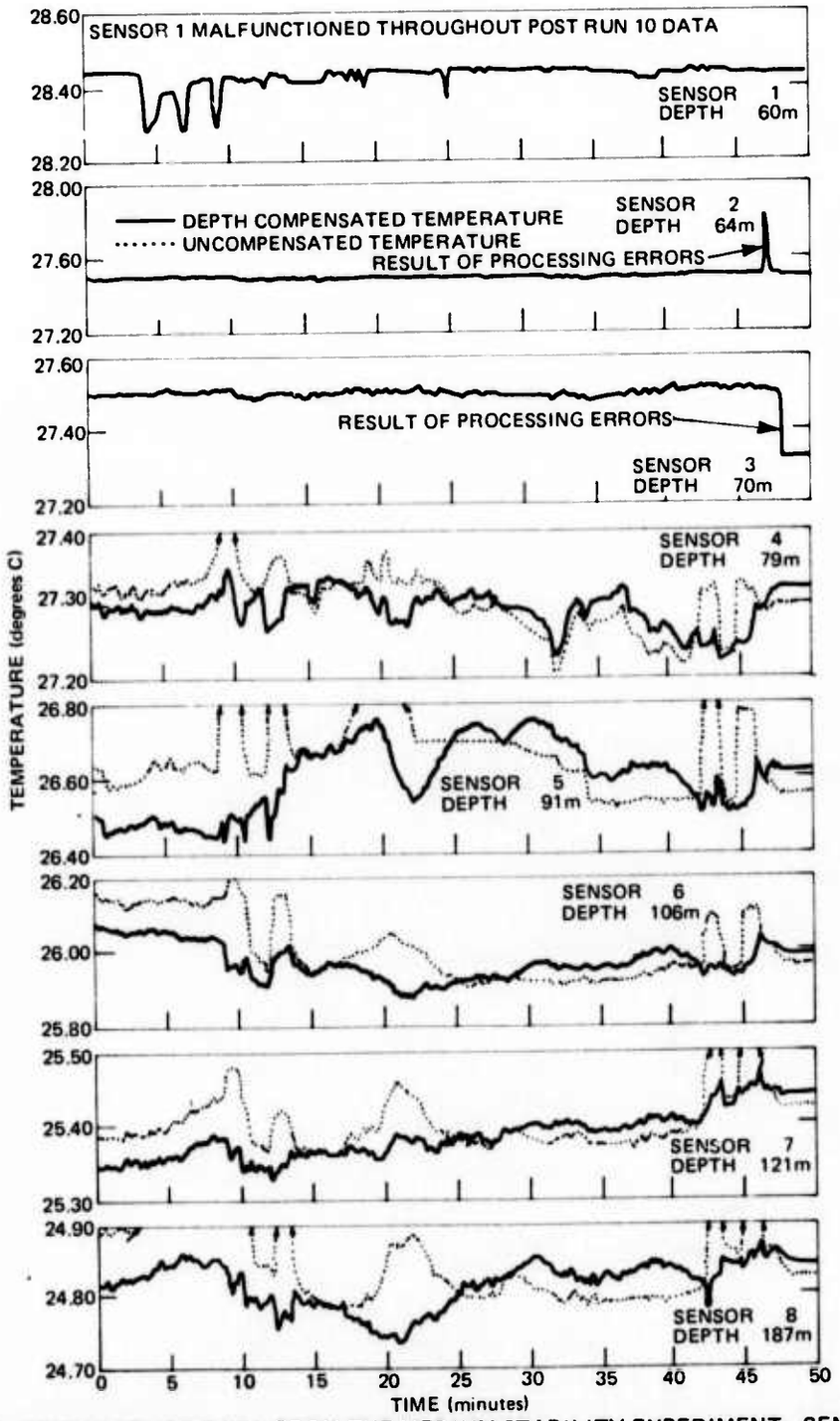

Fig. 13 TEMPERATURE DATA FROM THE MEDIUM STABILITY EXPERIMENT: SENSORS 1 THROUGH 8 (POST RUN 10, AUTEC, 5 NOVEMBER 1972; START TIME, 8:35:52Z)

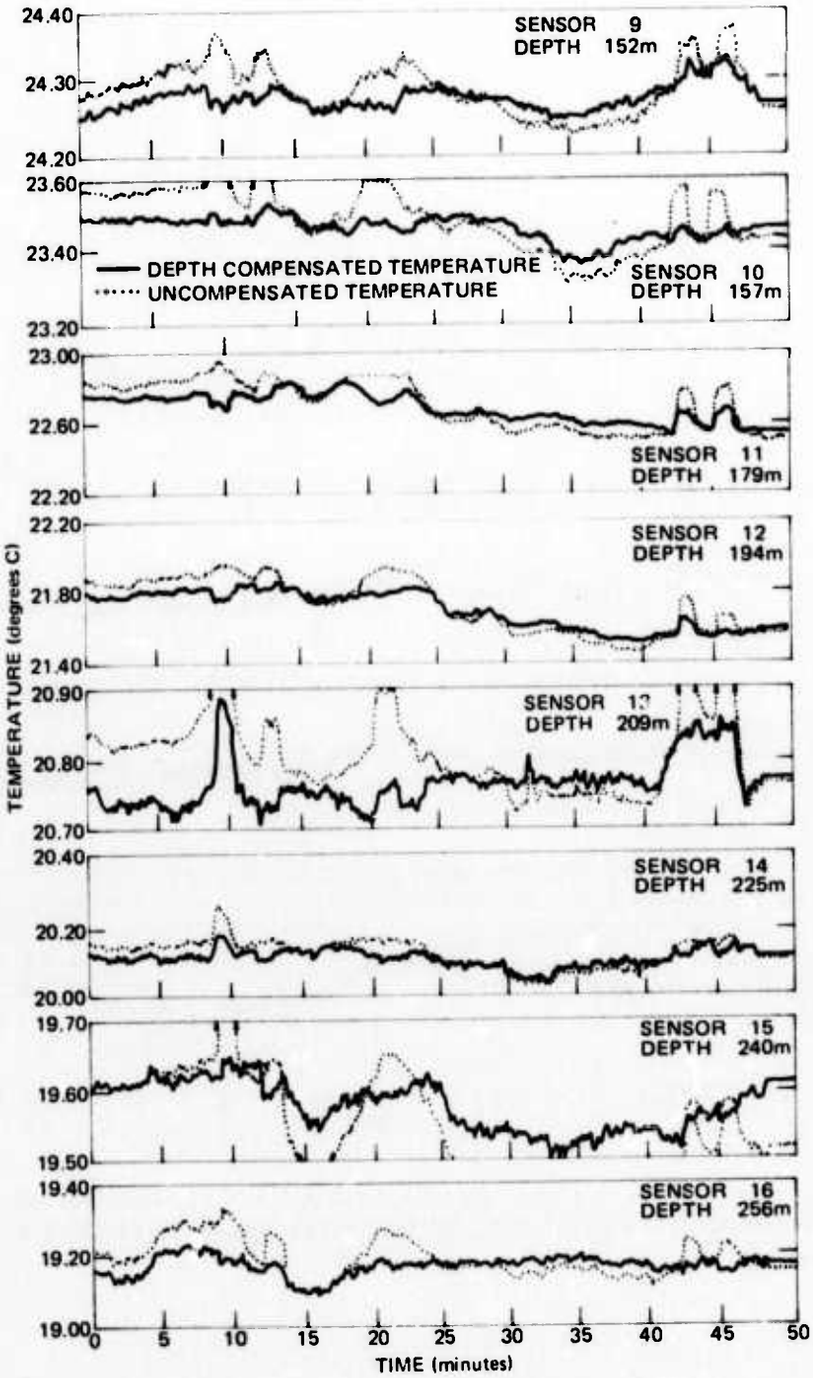

Fig. 14 TEMPERATURE DATA FROM THE MEDIUM STABILITY EXPERIMENT: SENSORS 9 THROUGH 16. (POST RUN 10, AUTEC, 5 NOVEMBER 1972; START TIME, 8:35:52Z)

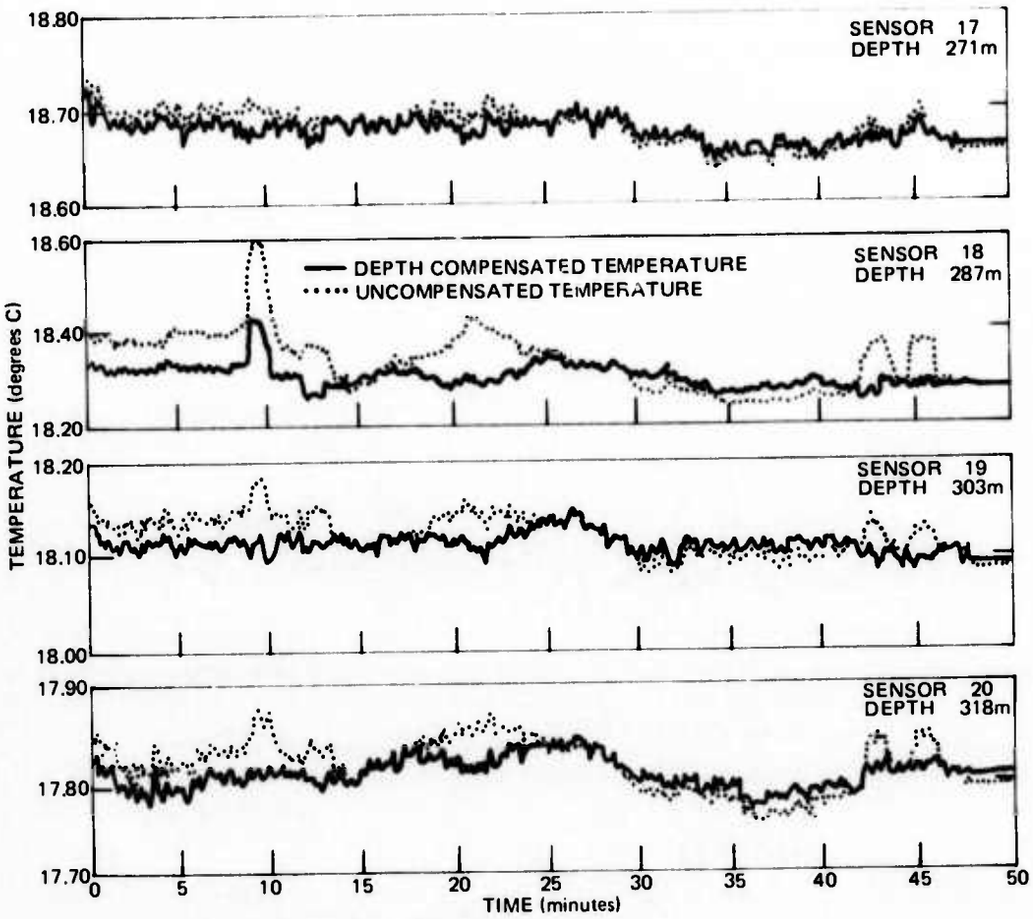

Fig. 15 TEMPERATURE DATA FROM THE MEDIUM STABILITY EXPERIMENT: SENSORS 17 THROUGH 20. (POST RUN 10, AUTEC, 5 NOVEMBER 1972; START TIME, 8:35:52Z)

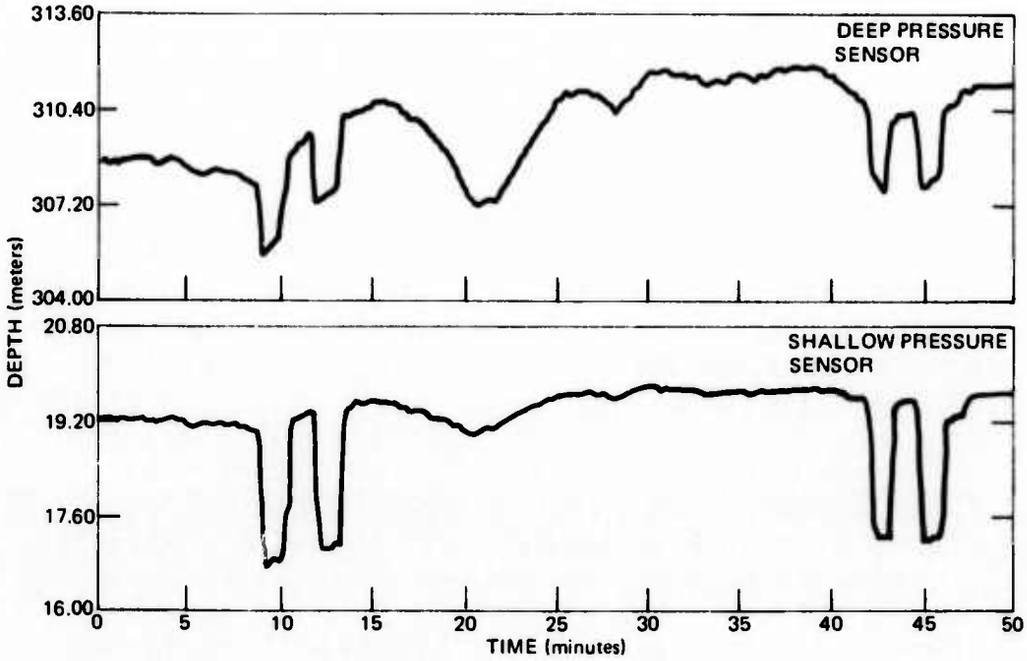

Fig. 16 DEPTH HISTORY OF DEEP PRESSURE AND SHALLOW PRESSURE SENSORS. (POST RUN 10, AUTEC, 5 NOVEMBER 1972)

from 3:30 to 5:00 a.m. local time in calm seas (sea state between 0 and 1) with a light breeze during a warm pristine November night off the Bahamas, the tranquility interrupted only by the occasional grey hulk of a shark circling the array.

The temperature and pressure data were recorded and compensated in the same manner as the data from Run 1. However, the array was raised and lowered several times during the run to establish the local temperature gradient about each sensor. Four of these raise and lower cycles are evident in the depth history (Fig. 16) of the array at times of 9.5 12.5, 43, and 46 minutes. During these cycles the array was gradually raised 2 1/2 meters, the new depth was maintained for 1 minute, and then the array was gradually lowered to its original depth. A single empirical temperature gradient for each sensor was determined from the raise-lower cycles and was used to compensate the recorded temperature data for the entire 50 minutes of processed post-Run 10 data. These gradients are shown as dots in Fig. 4 with the solid curve serving as a visual aid to connect the points.

Once again, the constant gradient approximation failed for some of the sensors some of the time. For instance, the compensated temperature derived from the output of sensor 13, which was positioned in a strong thermocline at 210 meters, shows a definite jump corresponding to the first raise-lower cycle at 10 minutes but no appreciable change during the second cycle 3 minutes later. There is no unequivocal evidence of internal waves in the data. However, there is a gradual decrease of the compensated temperature on sensors 10 through 12 and sensors 14 through 15 over a time span of 30 minutes, but these changes coincide with a gradual increase in depth of the array during the same period.

The temperature data for Run 3 were taken about 6 p.m. local time on the same day that the data from Run 1

were recorded. By that time the sea state was between zero and one, the seas were rising, and the breeze was about 5 knots. A typical temperature history for Run 3 is shown in Fig. 17 and the related pressure sensor histories are shown in Fig. 18. Even though the recorded temperature varied by more than 1°C during the run, the compensated temperature varied by no more than 0.1°C. However, the compensated temperatures for some of the sensors evidenced substantial changes that correlated with changes in depth of the array. These changes occurred because the spline profiles described in Chapter 4 were based on temperature measurements separated by 15 meters and were not sufficiently accurate to allow precise temperature compensation. Any evidence of internal waves was masked by changes of the depth of the array during Run 3.

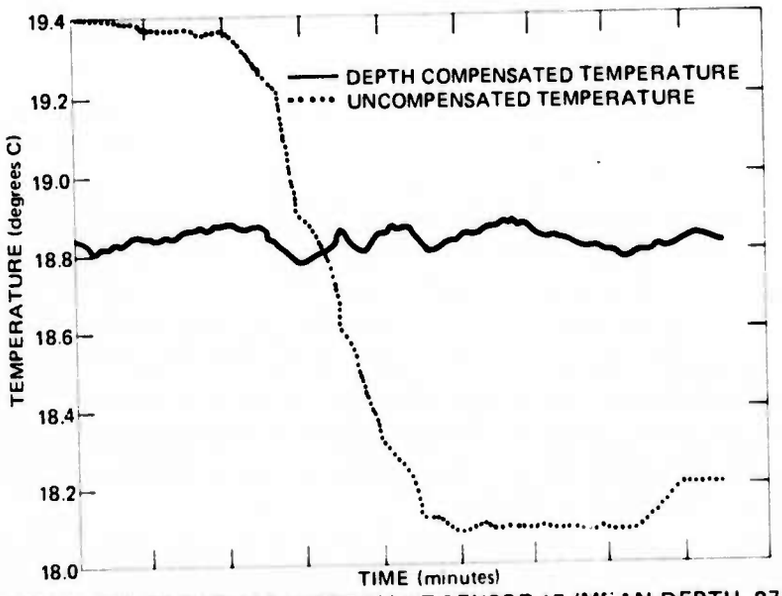

Fig. 17 TYPICAL TEMPERATURE HISTORY AT SENSOR 17 (MEAN DEPTH, 271 METERS). (RUN 3, AUTEC, 30 OCTOBER 1972; START TIME, 0:22:52Z)

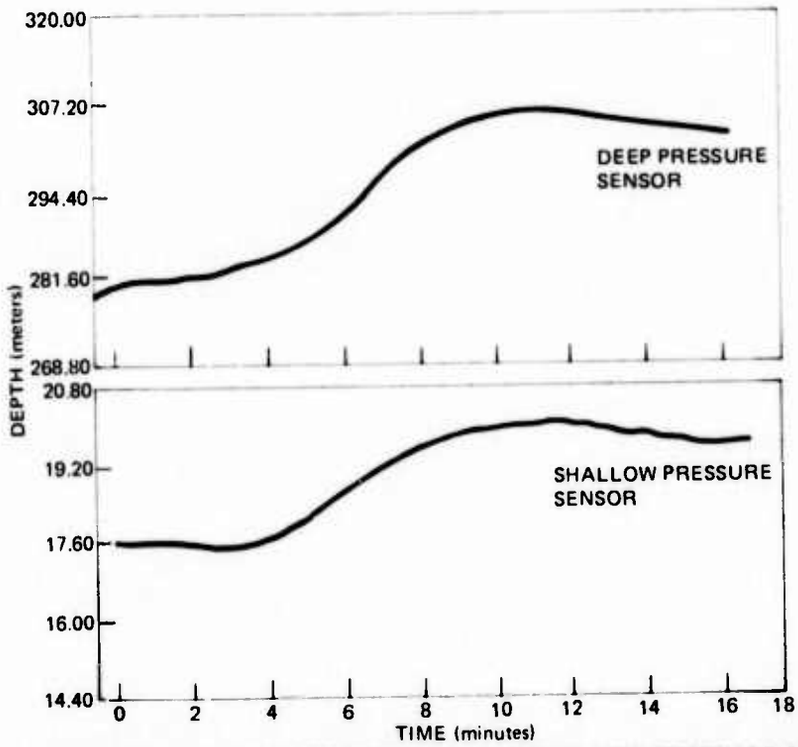

Fig. 18 DEPTH HISTORY OF DEEP PRESSURE AND SHALLOW PRESSURE SENSORS. (RUN 3, AUTEC, 30 OCTOBER 1972)

7. ACOUSTIC PATH-LENGTH STABILITY

If the density of seawater varies with time along an acoustic path ℓ, the velocity of sound c is modulated along that path. Consequently, the travel time $t = \ell/c$ of successive acoustic pulses traveling along the path will differ according to $\Delta t = -\frac{\ell}{c^2}\Delta c$, where Δt and Δc are the changes in travel time and sound velocity, respectively. Fluctuations in travel time can be expressed in terms of path length fluctuations $\Delta\ell$, according to

$$\Delta\ell = c\Delta t = -\frac{\ell}{c}\Delta c \ . \tag{4}$$

According to Ref. 7, an empirical expression for sound velocity as a function of temperature is given by

$$c = 1449 + 4.6T - 0.055\,T^2 + 0.0003T^3 + 0.017D + (1.39 - 0.012T)(S - 35)\ , \tag{5}$$

where c is in meters/sec, T is in °K, D is depth in meters, and S is salinity in parts per thousand. The sound velocity is predominantly a function of temperature although there is a slight dependence on salinity and pressure. For typical salinities on the order of 35 ppt the last term in Eq. 5 does not significantly affect the change of sound velocity with temperature. In this case the change in sound velocity can be expressed as

$$\Delta c \approx (4.6 - 0.11T + 0.0009T^2)\,\Delta T. \tag{6}$$

Ref. 7. L. Liebermann, "The Effect of Temperature Inhomogeneities in the Ocean on the Propagation of Sound," J. Acoust. Soc. Am., Vol. 23, 1951, p. 563

For temperatures on the order of 20°C, the change of sound velocity with temperature is approximately 2.5 meters/sec/°C.

By substituting Δc from Eq. 6 into Eq. 4, the path length fluctuations $\Delta \ell$ are easily expressed as a function of the temperature fluctuations ΔT. If the path length fluctuations $\Delta \ell_i(\Delta T)$ for the 19 paths lying between the 20 temperature sensors are summed coherently, the magnitude of the acoustic path length fluctuations for successive acoustic pulses traveling from the top to the bottom of the array is found to be

$$\Delta \ell = \sum_{i=1}^{19} \Delta \ell_i (\Delta T_i), \tag{7}$$

where ΔT_i is the average temperature change over the interval between the ith and ith + 1 sensor. The quantity ΔT_i is given by

$$\Delta T_i = \frac{1}{2} (T_i + T_{i+1} - R_i - R_{i+1}),$$

where R_i is an arbitrary reference temperature for the ith sensor from which changes in temperature are measured. The acoustic path length fluctuation computed from Eq. 7 is shown in Fig. 19 for Run 1 and the corresponding standard deviation of these fluctuations over 1 minute intervals is given in Fig. 20. The corresponding data for post-Run 10 are given in Figs 21 and 22 and the data for Run 3 are given in Figs. 23 and 24. Note that a 0.01°C temperature change across the 255-meter length of the array results in a change of about 4 millimeters in acoustic path length according to a straight forward application of Eq. 4.

Many of the features of the temperature and depth histories are apparent in the associated plot of path length fluctuations. For instance, the sudden increase in path length at 6.5 minutes in Fig. 19 is due to the missynchonization of the data processing algorithm with the temperature

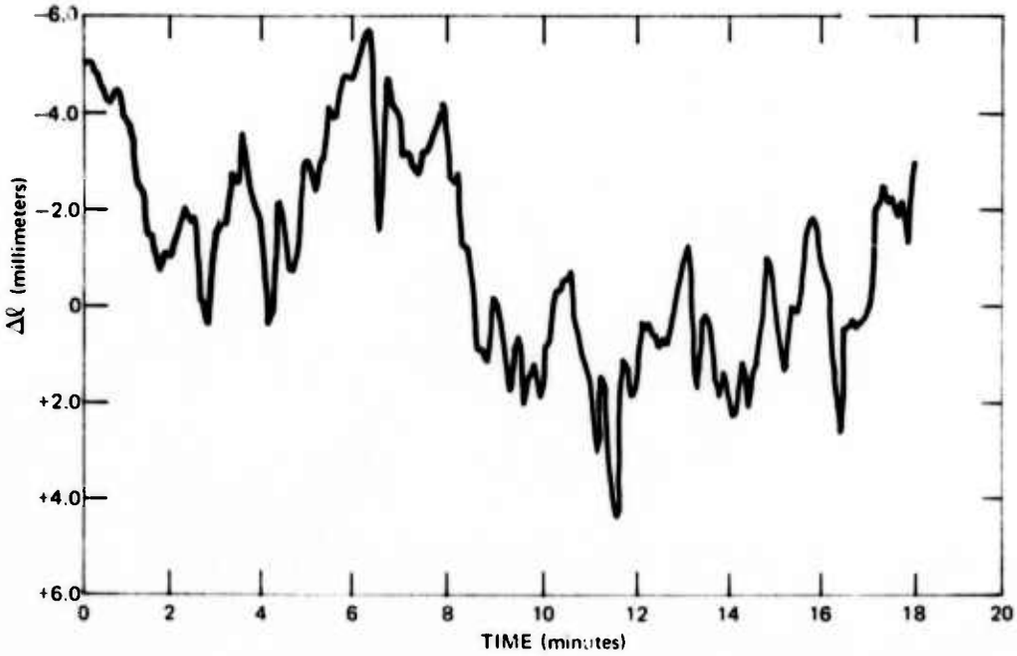

Fig. 19 VARIATION OF ACOUSTIC PATH, ℓ, WITH TIME OVER A 255-METER VERTICAL PATH. (RUN 1, AUTEC, 30 OCTOBER 1972)

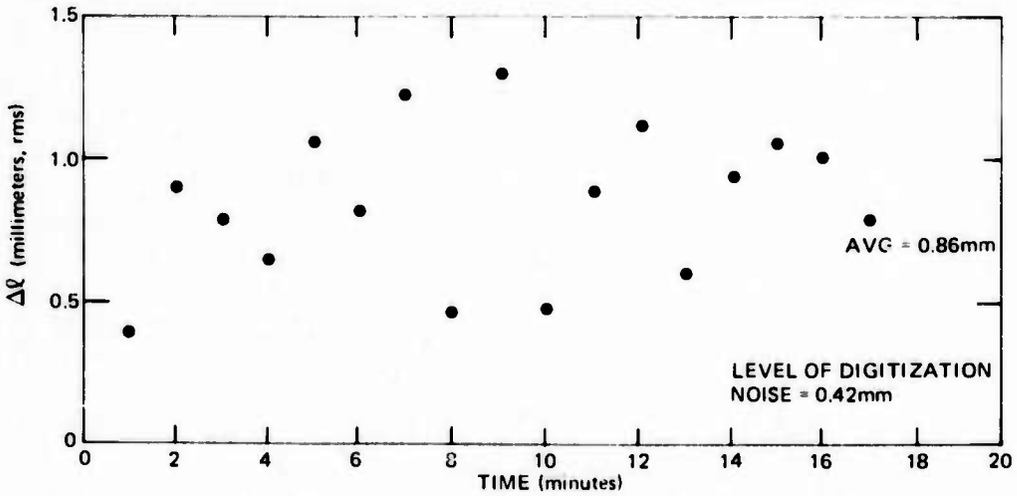

Fig. 20 STANDARD DEVIATION OF ACOUSTIC PATH-LENGTH FLUCTUATIONS COMPUTED OVER 1-MINUTE INTERVALS FOR A 255-METER PATH. (RUN 1, AUTEC, 30 OCTOBER 1972)

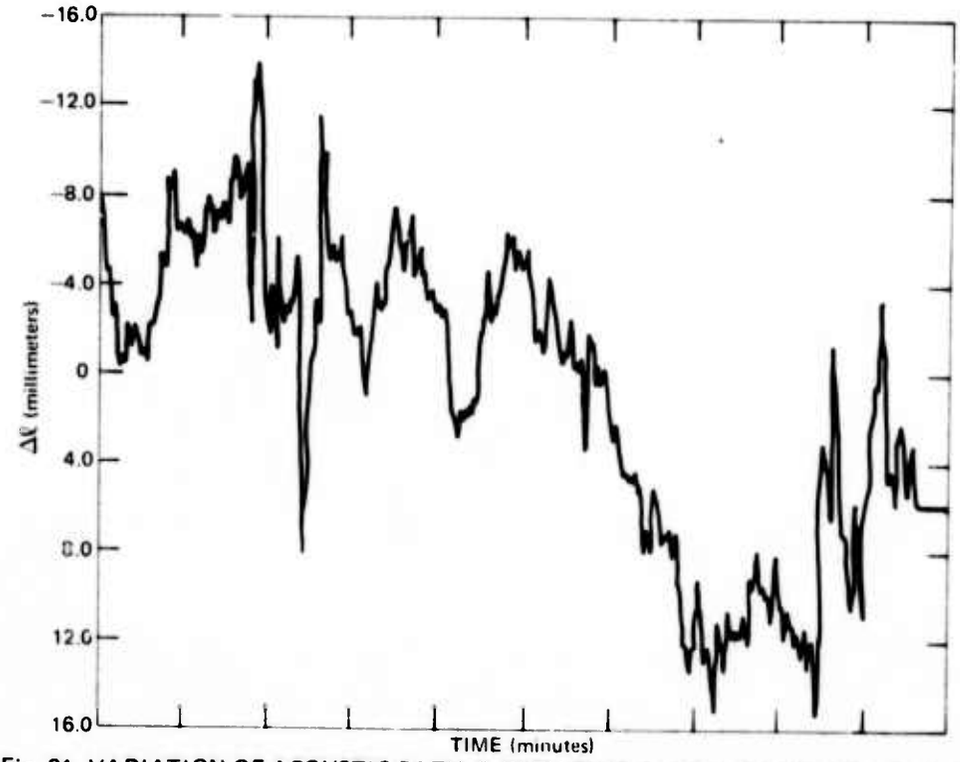

Fig. 21 VARIATION OF ACOUSTIC PATH, ℓ, WITH TIME OVER A 255-METER VERTICAL PATH. (POST RUN 10, AUTEC, 5 NOVEMBER 1972)

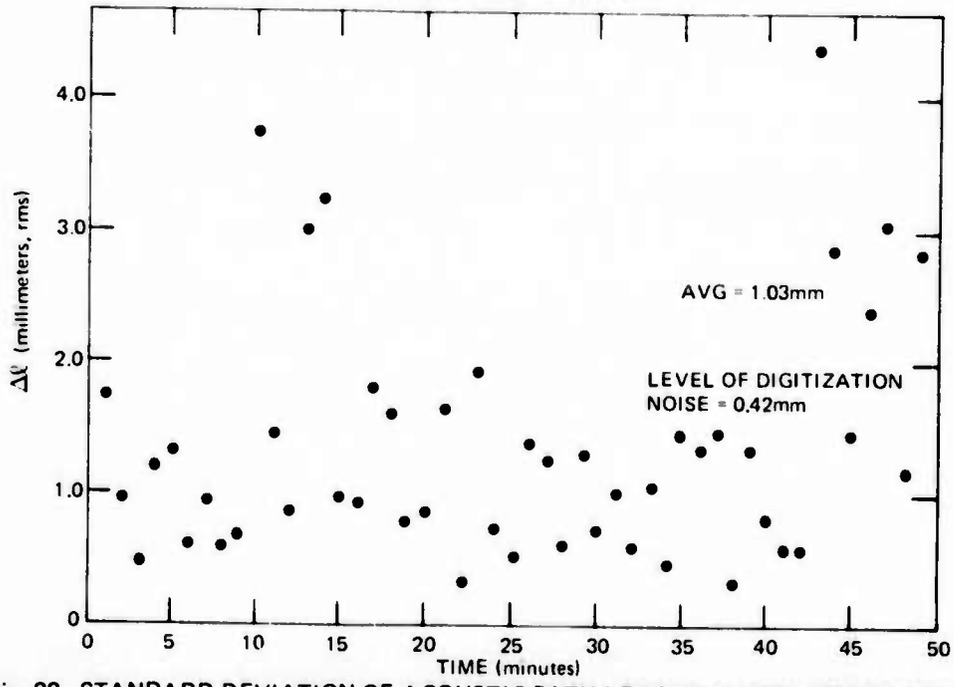

Fig. 22 STANDARD DEVIATION OF ACOUSTIC PATH-LENGTH FLUCTUATIONS COMPUTED OVER 1-MINUTE INTERVALS FOR A 255-METER PATH. (POST RUN 10, AUTEC, 5 NOVEMBER 1972)

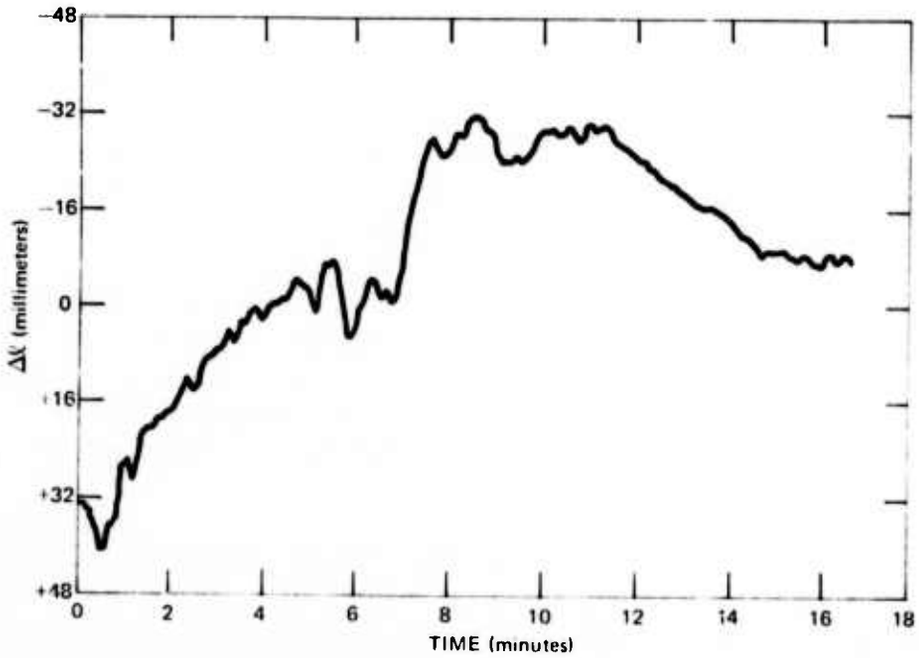

Fig. 23 VARIATION OF ACOUSTIC PATH, ℓ, WITH TIME OVER A 255-METER VERTICAL PATH. (RUN 3, AUTEC, 30 OCTOBER 1972)

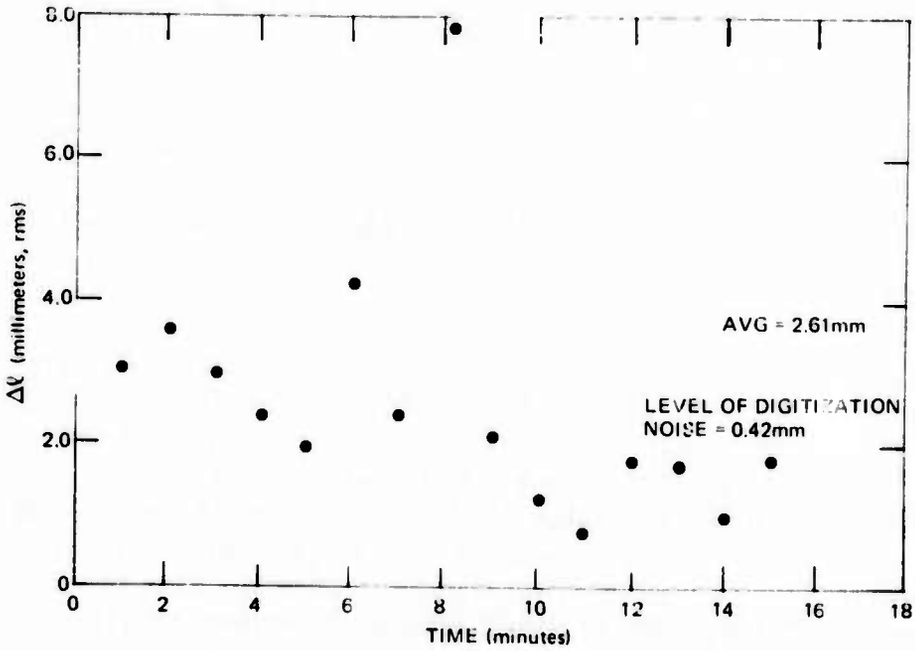

Fig. 24 STANDARD DEVIATION OF ACOUSTIC PATH-LENGTH FLUCTUATIONS COMPUTED OVER 1-MINUTE INTERVALS FOR A 255-METER PATH. (RUN 3, AUTEC, 30 OCTOBER 1972)

scanner as mentioned in Chapter 6. Similarly, the spikes occurring in the post-Run 10 data in Fig. 21 coincide with the raise-lower cycles of the array during the run. These spikes occur because the response time of the temperature sensors was much greater than that of the pressure sensors used to compensate for changes in depth.

During Run 3 the path length varied more than it did during the other two runs and this variation correlates appreciably with the depth history of the array (Fig. 18). This correlation is further evidence that the temperature compensation using the spline technique discussed in Chapter 4 was inadequate.

The slow variation of the path length observed in the Run 1 and post-Run 10 data may be due to internal waves or to cumulative path length errors. However, during minutes 6 through 12 of Run 1 no sensor changed its depth by more than 0.3 meter (Fig. 19). A depth error with a magnitude of 0.3 meter corresponds to path length errors of 3 millimeters in contrast to the observed 7-millimeter path length variation, which has an approximate period of 10 minutes. Similarly, during minutes 30 through 40 of the post-Run 10 data no sensor changed its depth by more than 0.6 meter (Fig. 21), but the path length varied by 10 millimeters during this time. For comparison, an internal wave with a 1-meter amplitude and with a wavefront extending across a region 50 meters in depth will cause changes in path length of 8 millimeters if the region has a temperature gradient of 0.04°C/meter.

The root mean square path length fluctuations during Run 1 and post-Run 10 are of the order of 1 millimeter when averaged over 1-minute intervals, as seen in Figs. 20 and 22. Appreciably larger values occurred during the raise-lower cycles in the post-Run 10 data. The average rms fluctuation level during Run 3 (Fig. 24) was 2.6 millimeters and is larger than the values from the other runs because of inadequate compensation of the temperature for depth variations.

The observed rms fluctuations are larger than the rms fluctuations due to digitization noise, by a factor of two, indicating that other measurement noise (e.g., temperature compensation) or genuine ocean path length fluctuations contributed to the observed rms values. In any case, a 1-millimeter rms upper bound can be placed on the acoustic path length fluctuations of a 255-meter path in the upper ocean, where the rms value is computed over 1-minute intervals. This upper bound is quite small, indicating that the ocean is a relatively stable acoustic medium over time periods of 1 minute. Based on these results, an acoustic signal with a frequency of 200 kHz would experience no more than a 1/8 wavelength perturbation due to ocean path length fluctuations, while propagating across the 255-meter region measured with the array.

Several qualifications should be placed on the 1-millimeter rms upper bound of the acoustic path length fluctuations. First, the temperature data were recorded with a sensor that had a response time of 3 1/2 seconds. Thus, contributions from fluctuations with periods less than the response time were not included in the computation of path length stability even though such fluctuations may be significant over short time periods. Our measurements provide an upper bound on low frequency variations of acoustic path length, such as might be caused by large scale turbulence or inhomogeneities with scale sizes on the order of meters.

The second qualification is that the temperature measurements were taken at discrete depths rather than across the continuum of depths that contribute to the path length stability of an acoustic signal. Consequently, our estimates of path length stability are only valid to the extent that the temperature histories at discrete depths are characteristic of the temperature variations across the continuum of depths.

In addition to characterizing the acoustic stability of the ocean by path length fluctuations, the stability can also be characterized by the related quantity μ, which is the ratio

of the change in the local sound velocity to the sound velocity itself; i.e.,

$$\mu = \Delta c / c. \tag{8}$$

The rms value of μ was derived from the temperature data for minutes 6 through 12 of Run 1 and minutes 30 through 39 of the post-Run 10 data. These times correspond to periods during which the depth of the array remained relatively constant. The measured values of μ showed no variation with depth nor any correlation with the magnitude of the temperature gradient such as would be expected if the gradient was a significant source of error. However, during both runs the rms value of μ was twice as large for the bottom 10 sensors than for the top 10, suggesting that more processing noise was introduced into the channel corresponding to the deep sensors than into the shallow channel. The rms value of μ for the 10 shallow sensors was 6×10^{-6} during both runs and the corresponding value of μ for the 10 deep sensors was 1.1×10^{-5}.

8. COMPARISON WITH OTHER MEASUREMENTS

During the Medium Stability Experiment, path length fluctuations were observed by acoustic techniques (Ref. 2), concurrently with the temperature measurements. The acoustic measurements showed path length fluctuations of 1.5 millimeters over a 2500-meter path. The frequency response of the acoustic measurements was essentially unlimited, whereas the temperature measurements were limited by the 3.5-second response time of the sensors. In both cases, the sampling rate was sufficiently slow that some of the high frequency fluctuations were aliased to lower frequencies.

The rms fluctuations derived from the acoustic measurements are of the same order as those derived from the temperature measurements, even though the path length was nearly 10 times as long. Both measurement techniques appear to be limited by measurement noise rather than ocean path length fluctuations. Thus, the variation in observed fluctuation levels obtained with the two techniques is indicative of the relative measurement noise rather than of the variation of cumulative ocean fluctuations with distance. No significant cross correlation of path length fluctuations was observed between the acoustic and temperature data.

Other investigators have also attempted to deduce path length stability from ocean temperature measurements. Lieberman (Ref. 7) measured temperature fluctuations with a sensor mounted on a submarine cruising at a constant depth between 30 and 60 meters off the California coast. He observed rms values for μ (Eq. 8) equal to 7×10^{-5}, using a thermometer with a response time less than 0.01 second. Urich (Ref. 8) describes a similar experiment in which

---

Ref. 8. R. J. Urich, Principles of Underwater Sound for Engineers, McGraw-Hill Book Co., New York, 1967, p. 151.

Urich and Searfoss found $\mu \approx 3 \times 10^{-5}$ using a sensitive submarine-mounted thermopile at a 7-meter depth off the coast of Florida. The rms values of μ obtained in these two experiments are larger by a factor of 5 to 10 than the value of 6×10^{-6} obtained with the upper 10 temperature sensors during the Medium Stability Experiment.

9. SUMMARY AND CONCLUSIONS

The temperature measurement program detailed in this report was part of the Medium Stability Experiment (Ref. 2) conducted at AUTEC in the Bahamas in the fall of 1972. Using a temperature array comprised of 20 thermistors and two depth sensors, ocean temperature profiles were measured as a function of time over the depth interval from 60 meters to 315 meters.

Fluctuations of the depth-compensated temperatures showed that acoustic path length fluctuations of the ocean were no more than 1 millimeter rms over periods of 1 minute. These measurements were taken over a 255-meter path and were only sensitive to fluctuations with a frequency of less than 1/3 Hz.

The 1-millimeter rms upper bound on path length fluctuations observed at AUTEC is equal to $\lambda/8$ for a 200-kHz acoustic signal. Based on these measurements, low frequency path length fluctuations were sufficiently small that coherent acoustic processing would have been possible at AUTEC with frequencies as high as 200 kHz over the 255-meter interval covered by the temperature array.

Path length fluctuations can be expected to increase as the square root of the range if ocean inhomogeneities are distributed stochastically. Nonetheless, at ranges exceeding 1/4 kilometer the maximum frequency of most physical systems will be limited by round-trip absorption losses rather than low frequency path length instabilities. Fluctuations including frequencies greater than 1/3 Hz were measured during the acoustic portion of the Medium Stability Experiment and were shown to be less than 1.5 millimeters over a 2500-meter path (Ref. 2).

ACKNOWLEDGMENTS

The temperature measurement program within the Medium Stability Experiment was brought to a successful conclusion through the cooperation and assistance of many APL personnel. Special assistance was provided by Dr. L. H. Wallman and Mr. B. E. Raff in rendering the equipment functional and in gathering data. Dr. D. C. Wenstrand provided competent analysis of the data associated with the Brünt-Väisälä frequency. Mr. R. J. McConahy and Mrs. B. J. Hook provided essential support in the numerical analysis of the data.

This work was supported by the Advanced Research Projects Agency under ARPA Order AO 1853 as part of a study to determine the scientific feasibility of applying synthetic aperture processing techniques in an ocean environment.

Preceding page blank

REFERENCES

1. A. J. Tardif (ed.), Synthetic Aperture Sonar Medium Stability Experiment, Raytheon Company, Submarine Signal Division, 1973.

2. D. W. Stowe, L. H. Wallman, J. W. Follin, Jr., and P. J. Luke, Stability of the Acoustic Path Length of the Ocean Deduced from the Medium Stability Experiment, APL/JHU TG 1230, January 1974.

3. A. Hald, Statistical Theory with Engineering Applications, John Wiley and Sons, Inc., New York, 1965, p. 199.

4. H. Schlichting, Boundary Layer Theory (6th Edition), McGraw-Hill Book Co., New York, 1968, pp. 9-16.

5. J. H. Ahlberg, E. N. Nilson, and J. L. Walsh, The Theory of Splines and Their Applications, Academic Press, New York, 1967.

6. O. M. Phillips, The Dynamics of the Upper Ocean, Cambridge University Press, Cambridge, Mass., 1966, p. 162.

7. L. Liebermann, "The Effect of Temperature Inhomogeneities in the Ocean on the Propogation of Sound," J. Acoust. Soc. Am., Vol. 23, 1951, p. 563.

8. R. J. Urich, Principles of Underwater Sound for Engineers, McGraw-Hill Book Co., New York, 1967, p. 151.

Preceding page blank

Appendix

CALCULATION OF ARRAY CONFIGURATION

In the absence of boat motion and ocean currents the temperature array will hang vertically in the water. However, if the array moves with respect to the water, it assumes a curved orientation due to the hydrodynamic drag acting on the array.

According to Ref. 4, an object experiences a drag δ in the direction of motion given by

$$\delta = \frac{1}{2}\rho V^2 C A_N, \tag{A-1}$$

where ρ is the density of the medium, V is the velocity of the object, C is the appropriate drag coefficient, and A_N is the projection of the area of the object in the direction of motion. For the geometries and velocities appropriate to the Medium Stability Experiment, the cross section of the array approximates a right circular cylinder with a drag coefficient of 1.2 (Ref. 4). The lift component of drag is neglected in this treatment because the array hangs nearly vertical.

Since the length of the array is much greater than its diameter D, it is convenient to consider the drag acting on a short segment $\Delta\ell$ of the array. The array is assumed to move horizontally with a velocity $\vec{V}$ through a motionless ocean. As illustrated in Fig. A-1, a length $\Delta\ell$ of the array has a projected area in the direction $\vec{V}$ equal to $\Delta A_N = D\Delta\ell \cos\theta$, where θ is the inclination of the array with respect to the vertical. When this expression for the projected area is substituted into Eq. A-1, the drag $\Delta\delta$ acting on the segment $\Delta\ell$ of the array is found to be

$$\Delta\delta = \frac{1}{2}\rho V^2 C \Delta A_N = \frac{1}{2}\rho V^2 CD \cos\theta\, \Delta\ell.$$

Pages 64, 65 + 66 are Blank.

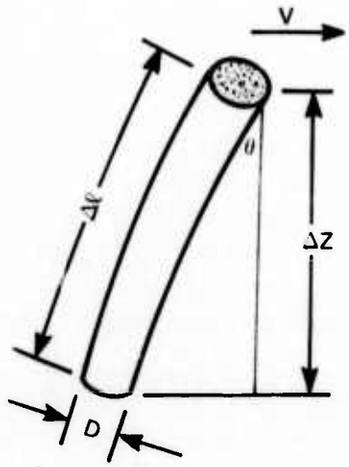

THE PROJECTED AREA IN THE DIRECTION OF $\vec{V}$ IS $\Delta A_N = D\Delta\ell \cos\theta$

Fig. A-1 PROJECTED AREA OF A SEGMENT OF THE TEMPERATURE ARRAY

The horizontal component of the array tension T_x varies in such a manner that the difference T_x between two nearby points, 1 and 2, is just equal to the drag acting on the array between those points. This relationship is depicted in Fig. A-2 and can be expressed in the form

$$\frac{T_{x_2} - T_{x_1}}{\Delta \ell} = -\frac{\Delta \delta}{\Delta \ell} = -\frac{1}{2}\rho V^2 CD \cos \bar{\theta}, \qquad \text{(A-2)}$$

where $\theta_2 < \bar{\theta} < \theta_1$ and where θ_1 and θ_2 are the angles of inclination of the array at the two points. In the limit as $\Delta \ell \to 0$ Eq A-2 becomes

$$\frac{dT_x}{d\ell} = -\frac{1}{2}\rho V^2 CD \cos \theta, \qquad \text{(A-3)}$$

where $\theta_1 \to \bar{\theta} \to \theta_2 = \theta$.

If a sinker of weight mg is affixed to the lower end of the array, the vertical component of the tension T_z must satisfy

$$T_z = mg. \qquad \text{(A-4)}$$

Implicit in this expression is the assumption that the array itself is neutrally buoyant; i.e., the density of the array is the same as that of seawater.

The relationship between the horizontal and vertical components of tension is given by

$$T_x/T_z = \tan \theta. \qquad \text{(A-5)}$$

Taking the derivative of Eq. A-5 with respect to ℓ and substituting for T_x and T_z from Eq. A-3 and A-4, it follows that

$$\frac{1}{2}\rho V^2 CD \cos \theta = -mg \sec^2 \theta \frac{d\theta}{d\ell}. \qquad \text{(A-6)}$$

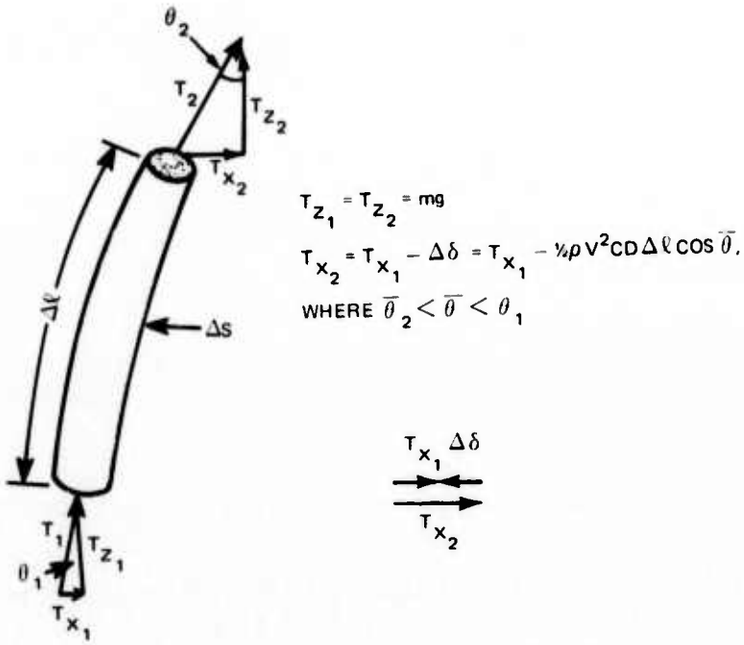

Fig. A-2 COMPONENTS OF TENSION IN A SEGMENT OF THE TEMPERATURE ARRAY

Recognizing that the horizontal and vertical displacement differentials are given by $dx = d\ell \sin\theta$ and $dz = d\ell \cos\theta$, Eq. A-6 can be expressed as

$$x = -\int_{o}^{\theta_o} \frac{mg}{\frac{1}{2}\rho V^2 CD} \frac{\sin\theta}{\cos^3\theta} d\theta \qquad \text{(A-7a)}$$

and

$$z = -\int_{o}^{\theta_o} \frac{mg}{\frac{1}{2}\rho V^2 CD} \frac{1}{\cos^2\theta} d\theta. \qquad \text{(A-7b)}$$

If the array diameter D is constant, then the Eqs A-7a and A-7b can be integrated in closed form to yield the relationship

$$x = BZ^2, \qquad \text{(A-8)}$$

where $B = \rho V^2 CD/4mg$. The horizontal displacement x and the vertical displacement z are measured from the bottom of the array. Eq. A-8 is the equation of a parabola with its directix parallel to the z-axis and its vertex at the bottom of the array.

The diameter of the array used at AUTEC was smaller near the bottom than near the top because fewer cables extended to the bottom. In this case the diameter can be approximated by a uniform taper proportional to the arc length of the cable.

$$D = D_o (1 + \alpha\ell).$$

Using this expression for the diameter, Eq. A-5 can be solved numerically to obtain the configuration of the array.

Sample calculations for a uniform diameter and a tapered diameter array are given in Fig. 5 of the text. The value of the coefficient B in Eq. A-8 can be determined empirically if the depth of the vertex of the array and the depth and arc length to another point on the array is given. During the Medium Stability Experiment this information was provided by the deep and shallow pressure sensors. Once the shape of the array is known, the arc length can be integrated numerically along the array to determine the depths of the temperature sensors.